# A New Self-Consistent Empirical Interatomic Potential Model for Oxides, Silicates, and Silica-Based Glasses

**Alfonso Pedone,[†] Gianluca Malavasi,[†] M. Cristina Menziani,[†] Alastair N. Cormack,[‡] and Ulderico Segre*,[†]**

*Department of Chemistry and SCS Center, University of Modena and Reggio Emilia, Via G. Campi 183, 41100 Modena, Italy, and Kazuo Inamori School of Engineering, New York State College of Ceramics, Alfred University, Alfred, New York 14802*

A new empirical pairwise potential model for ionic and semi-ionic oxides has been developed. Its transferability and reliability have been demonstrated by testing the potentials toward the prediction of structural and mechanical properties of a wide range of silicates of technological and geological importance. The partial ionic charge model with a Morse function is used, and it allows the modeling of the quenching of melts, silicate glasses, and inorganic crystals at high-pressure and high-temperature conditions. The results obtained by molecular dynamics and free energy calculations are discussed in relation to the prediction of structural and mechanical properties of a series of soda lime silicate glasses.

## 1. Introduction

Silica-based glasses are of great importance in the fields of both technological industries and geosciences. Fiber optic waveguides, laser optics for initiating fusion reactions, and containers for radioactive waste are recent developments that demonstrate the importance, versatility, and potentiality of glass for additional uses.[1]

Insight into composition–structure–property relationships is fundamental for designing new materials of technological importance and for gaining a better understanding of geological phenomena. Computational techniques such as perfect lattice calculations,[2] lattice dynamics[3] and molecular dynamics (MD) simulations[4] are useful tools for calculating physical chemistry properties. In fact, structural properties, elastic constants, high-frequency and static dielectric constants, refractive indices, heat capacities, thermal expansion coefficients, and other thermodynamic properties can be calculated nowadays at any temperature and pressure for both glasses and crystal solids.[5-7]

As it is well-known, interatomic potentials are of fundamental importance for the accuracy of the simulated properties. Several interatomic potentials are available in the literature for $SiO_2$ polymorphs and vitreous silica ($v$-$SiO_2$).[4,8-11] A Morse function was used successfully by Takada et al.[12] to study structural changes in cristobalite at high temperature and to simulate $v$-$SiO_2$. Kieffier et al.[7,13] successfully simulated the $\alpha$–$\beta$ phase transition in silica cristobalite and $v$-$SiO_2$ by means of a force field that included a Born–Huggins–Mayer two-body term, a three-body angular term, and charge–dipole and dipole–dipole interaction terms. -Goddard and co-workers[8,14] used a Morse function with configurationally dependent charges to study phase transition in silica polymorphs and $v$-$SiO_2$. The use of variable charge potential models, in which charges are determined according to the electronegativity equalization (QEq) scheme

of Rappe and Goddard,[15] proved to be a more appropriate method to study silicate structures and glasses in which the bond covalency changes with composition and instantaneous configurations. Unfortunately, MD codes in which this method has been implemented are limited by the computational effort required, and multicomponent glasses have not been studied with this method so far. Wilson et al.[16] successfully calculated the infrared spectrum for pure $v$-$SiO_2$ by means of a potential that includes formal ionic charges and an explicit account of polarization effects.[17] Their approach was more recently applied to the simulation of bulk and surface properties of amorphous $SiO_2$,[18,19] but no applications to multicomponent glasses have been reported. To improve the description of the inter-tetrahedral structure of the silicon network and of the local environment surrounding modifier cations, a potential for pure silica, sodium silicate, and soda lime silicate glasses that includes polarization effects through the shell model was recently developed.[20]

A more general force field, implemented into the Cerius2 and Material Studio packages,[21] was developed for multicomponent silicate glasses by Garofalini et al.,[22] who successfully studied bulk and surface structures and diffusion processes.

However, the potentials developed by Garofalini et al.[22] were derived empirically to model structural features, and their performances in calculating mechanical properties are poor. Moreover, despite the obvious interest in the modeling of different silicates, usually the researchers develop, from time to time, the parameters that they need for the system at hand, and a general force field for these materials is still lacking in the literature.

The aim of this work is to provide a generalized self-consistent force field able to model both structures and mechanical properties of silica-based glasses with different compositions. Zachariasen[23] claimed that atomic forces in glasses and in the corresponding crystals must be of the same order of magnitude, since the observed mechanical properties are similar. In this framework, it is reasonable to assume that a force field able to reproduce properties of silicate crystals can be also successfully used to simulate silica-based glasses, as

* Author to whom correspondence should be addressed. Phone: +39 059 2055095. Fax: +39 059 373543. E-mail: segre@unimo.it.
† University of Modena and Reggio Emilia.
‡ Alfred University.

Empirical Interatomic Potential Model for Glasses

*J. Phys. Chem. B, Vol. 110, No. 24, 2006* **11781**

the deviation in the intermediate range order from crystal phases is mainly due to the cooling procedure applied in the simulation.

On one hand, obtaining parameters for a single crystal phase does not ensure their transferability to the other classes of silicates, but on the other hand, because of the great variety of silicate classes, to fit parameters on all of the crystals simultaneously is not feasible.

Therefore, we have derived a set of interatomic pairwise potentials for binary oxides, which are subsequently transferred to the silicate systems. Potentials developed to study oxides are available in the literature[24,25] and have been widely used in combination with the well-known Vessal's potentials[26] to model structural features in multicomponent glasses.[27-32] However, all these potentials were derived from fitting the calculated structure and properties at $T = 0$ K to experimental data at 300 K.

To produce a coherent set of potential functions, we have performed empirical fitting to structural and, when available, mechanical properties of a large set of oxides. Thermal quasi-harmonically and zero-point motion effects have been included by means of free energy minimization,[33] which is available within the GULP package.[34-37] The performance of this potential set has been tested in the prediction of structural and mechanical properties of a wide range of silicate crystals and of series of sodium silica glasses. Moreover, the reliability of the force field in modeling alumino-phosphate has been ascertained by comparing the computed structural and mechanical properties of $AlPO_4$ berlinite with those calculated with other potential models.[38,39]

## 2. Methodology

**2.1. Interatomic Potential Derivation.** The empirical fitting method implemented in the GULP package[34-37] has been used to derive the interatomic potential parameters. In this method, the parameters are derived to reproduce the experimental crystal structures (lattice parameters and atomic positions for one or more configurations) and/or crystal properties that contain information concerning the shape of the energy surface, such as elastic constants, high-frequency and static dielectric constants, lattice energy, piezoelectric constants, or phonon frequencies.

The conventional fitting procedure consists of the following steps:

(1) The structural crystal properties and the initial guess for the potential parameters are read.

(2) The six cell strains ($\epsilon(i)$, $i = 1, ..., 6$), internal strains ($\epsilon(i,j)$, $i = 1, ..., N$, $j = x, y, z$), and properties ($C_{obs}(l)$, $l = 1, ..., M$) of the initial structures are calculated with the guess potentials.

(3) The weighted sum of squares is calculated according to

$$F = \sum_{i=1}^{6} \omega_{1i}\epsilon(i)^2 + \sum_{i=1}^{N}\sum_{j=1}^{3} \omega_{2ij}\epsilon(i,j)^2 +$$
$$\sum_{l=1}^{M} \omega_{3l}(C_{calc}(i) - C_{obs}(i))^2 \quad (1)$$

where $\omega_{1i}$, $\omega_{2ij}$, and $\omega_{3l}$ are the weighting factors that control the contribution of each term to $F$. The choice of the weighting factor value for each observable depends on the reliability and the precision of the experimental methods used for its determination.

(4) The value of $F$ is minimized by varying the potential parameters. The procedure stops when the energy gradients for all atoms (i.e., the forces acting on them) are below a definite value.

It may happen that the minimization of forces sometimes leads to a worse structure. This can occur because in a harmonic approximation the displacements in the structure are given by the gradient vector multiplied by the inverse of the Hessian matrix. Hence, if the gradients get smaller but the inverse Hessian gets larger, then the displacements may get worse. Gale solved the problem by introducing the so-called relaxed fitting.[35] The main criterion used to estimate the accuracy of the potential model in the relaxed fitting method is given by the displacements of the computed structure away from the experimental configuration instead of the forces values at the experimental geometry. This means that the structure is optimized at every step in the fit and the displacements of the structural parameters are calculated instead of the energy gradients. Assuming that the local energy surface is quadratic, the displacement vector $\Delta$ is given by

$$\Delta = -\mathbf{H}^{-1} \cdot \mathbf{g} \quad (2)$$

where $\mathbf{H}$ is the Hessian matrix and $\mathbf{g}$ is the gradient vector.

In many cases, the potentials reported in the literature were derived by fitting calculated structures and properties at $T = 0$ K to experimental data obtained at 300 K. A more rigorous treatment requires that in the fitting method each observable is calculated at the temperature corresponding to the empirical data being employed. This implies that properties and crystal structures must be calculated by considering thermal forces. In fact, the temperature is explicitly included in the GULP code by means of the free energy minimization method.[33] In this work we have used the latter method, at finite temperature and pressure, in conjunction with relaxed fitting. Details on Gibbs free energy minimization can be found elsewhere.[40]

The elastic constants, at specific temperature and pressure, are defined as the second derivative of the Gibbs free energy with respect to the strain components[41]

$$C_{ij} = \frac{1}{V}\left(\frac{\partial^2 G}{\partial \epsilon_i \epsilon_j}\right)_X \quad (3)$$

This can be calculated at constant temperature (isothermal $X = T$) or at constant entropy (adiabatic $X = S$).

**2.2. Potential Model.** In the recent years, pairwise potentials with partial charges have been extensively used. When partial charges are assigned to ions, as in the Beest−Kramer−Santen (BKS) model, the contribution of the dispersion term in the Buckingham function becomes important and the Buckingham potential assumes unphysical values at low internuclear distances.

This can be problematic when the temperature used in the simulation is high. Therefore, many authors add a repulsive term of the type $D/r^n$ to model the quenching of melts and glass formation.[30,42,43]

Three terms contributed to the potential used in this work: (a) long-range Coulomb potential, (b) short-range Morse function, and (c) repulsive contribution $C/r^{12}$, necessary to model the interaction at high temperature and pressure. Therefore, the expression for the resulting potential is given by

$$U(r) = \frac{z_i z_j e^2}{r} + D_{ij}[\{1 - e^{-a_{ij} \cdot (r-r_0)}\}^2 - 1] + \frac{C_{ij}}{r^{12}} \quad (4)$$

The Morse function is usually used in modeling bonded interactions in covalent systems (e.g., the hydroxide ion in ionic systems) in which the Coulomb term is subtracted. In this case

the physical meaning of the different quantities is well defined: $D_{ij}$ is the bond dissociation energy, $a_{ij}$ is a function of the slope of the potential energy well, and $r_0$ is the equilibrium bond distance. This is not the case here because the Coulomb term is explicitly included, and $D_{ij}$, $a_{ij}$, and $r_0$ should be simply considered as parameters.

A rigid ionic model with partial charges is used to handle the partial covalency of silicate systems. Given the success of the BKS potential,[6] the charge on the oxygen atom has been kept fixed at $q_O = -1.2e$. The partial charges on the cations are referred to the value of the oxygen charge for self-consistency of the force field. So, the silicon atom has a charge of $2q_O$, the alkaline ions of $0.5q_O$, and so on. It should be stressed again that these are "effective charges" and they must be treated as parameters in the potential model, and together with the short-range terms they form an "effective potential", although the physical significance of the individual terms may in some cases be uncertain.

The choice of the rigid ionic model is due to the aim of modeling the quenching of melts and structures and mechanical properties of glasses. In fact, a core−shell model should provide more accurate results for dielectric properties, surfaces, and defective crystals, but it requires a short time step in MD simulations, leading to cooling procedures for the quenching of melts that are computationally more expensive.

In this framework, the parameters for the functional form chosen have been derived from the binary oxide following the steps:

(a) The Si−O and O−O interactions have been conventionally fitted using the structural properties and the elastic tensor of α-quartz with the aim to obtain the initial guess parameters.

(b) The parameters obtained in the previous step have been refitted using relaxed fitting in conjunction with free energy minimization to take into account the effects of temperature and pressure ($T = 300$ K and $P = 1$ atm). The weighting factors have been increased to $10^4$, $10^5$, and 10 for lattice vectors, atom positions, and elastic constants, respectively.

(c) The cation−oxygen short-range interactions have been fitted for the binary oxides following points a and b, while the O−O interaction derived previously has been kept fixed. The Al−O parameters have been derived from the structural properties and elastic constants of α-corundum, the Mg−O ones from the MgO periclase observables, and so on.

(d) No elastic properties are available in the literature for alkaline oxides, and therefore, the number of parameters is greater than the number of observables, and a different parametrization is necessary. In these cases, the M−O parameters, with M = Li, Na, K, have been obtained by fitting the potential to silicates with the formula $M_2Si_2O_5$, with the Si−O interaction derived in point b fixed.

The Coulomb term in eq 4 is accurately evaluated through the Ewald summation.[44] In this work, the short-range potential cutoff has been set to 15 Å, the Newton−Raphson method[45] has been employed for minimization, and the approach of Fletcher and Powell[46] has been used to update the Hessian matrix.

**2.3. Computation of Elastic Constants.** The Gibbs free energy of each configuration has been minimized at room temperature and pressure, and the elastic compliance matrix has been calculated by the second derivative method of eq 3. Once the stiffness or elastic matrix **C** is obtained, several related mechanical properties of anisotropic materials can be derived

**TABLE 1: Molar Composition, Number of Atoms, Cell Sizes, and Densities of the $x$Na$_2$O−(100 − $x$)SiO$_2$ Simulated Glasses**[a]

| formulation | $x$ Na$_2$O | number of atoms in the simulation box | | | density (g/cm$^3$) | cell size (Å) |
|---|---|---|---|---|---|---|
| | | Na | Si | O | | |
| SiO$_2$ | 0 | 0 | 512 | 1024 | 2.200 | 28.5290 |
| NS10 | 10 | 102 | 461 | 973 | 2.294 | 28.1633 |
| NS15 | 15 | 154 | 435 | 947 | 2.340 | 27.9924 |
| NS20 | 20 | 204 | 410 | 922 | 2.385 | 27.8294 |
| NS25 | 25 | 256 | 384 | 896 | 2.428 | 27.6788 |
| NS30 | 30 | 308 | 358 | 870 | 2.469 | 27.5393 |

[a] The total number of atoms in each box is 1536.

from their matrix elements or from the matrix elements of the compliance matrix **S**

$$\mathbf{S} = \mathbf{C}^{-1} \quad (5)$$

In particular, the bulk modulus is calculated from the compliance matrix as follows

$$B^{-1} = S(1,1) + S(2,2) + S(3,3) + 2[S(3,1) + S(2,1) + S(3,2)] \quad (6)$$

and the values of the Young's modulus along three orthogonal directions are given by

$$E_k^{-1} = S(k,k) \quad k = 1, 3 \quad (7)$$

The number of independent elastic parameters depends on the symmetry of the crystalline material.[41] For isotropic materials the three principal values $E_k$ must be equal. Moreover, the Poisson ratio $\nu$ and the shear modulus $G$ are related to $B$ and $E$ by the equations

$$B = \frac{E}{3(1 - 2\nu)} \quad (8)$$

$$G = \frac{E}{2(1 + \nu)} \quad (9)$$

so that only two elastic constants are independent.

Elastic properties for glasses can be calculated and compared with experimental data[47,48] and with those calculated using different empirical methods.[49]

**2.4. MD Simulation of Sodium Silica Glasses.** The model potentials derived have been applied to the simulation of a series of sodium silica glasses. The $x$Na$_2$O−(100 − $x$)SiO$_2$ series of glasses with $x = 0$, 10, 15, 20, 25, and 30, which will be denoted as SiO$_2$, NS10, NS15, NS20, NS25, and NS30, respectively, have been considered. Densities at room temperature have been calculated with Appen's empirical method[47] to be 2.200, 2.294, 2.340, 2.385, 2.428, and 2.469 g/cm$^3$, respectively.

The glass structures have been modeled by Molecular Dynamics (MD) simulation by means of the DL_POLY package.[50] For each composition 1536 atoms have been placed in a cubic box with an edge length ranging from 27.41 to 28.53 Å (Table 1), and three simulations have been performed with different starting randomly generated configurations. Integration of the equation of motion has been performed using the Verlet Leapfrog algorithm with a time step of 2 fs. To minimize the computational effort without altering the accuracy of the calculations the short-range interaction cutoff has been set to 5.5 Å. The same cooling procedure successfully used in recent works[30,43] has been used. The systems have been cooled

Empirical Interatomic Potential Model for Glasses

*J. Phys. Chem. B, Vol. 110, No. 24, 2006* **11783**

uniformly from 5000 to 300 K, by decreasing the temperature with steps of 500 K. The total cooling time is 470 ps with 235 $\times 10^3$ time steps and a nominal cooling rate of $1 \times 10^{13}$ K/s. At each temperature a 20 000 time step relaxation has been allowed. During the first set of 6000 time steps, the velocity is scaled every time step. During the second set of 6000 time steps, velocity scaling every 40 time steps has been performed, and finally, during the last 8000 time steps, no velocity scaling was applied. The canonical ensemble NVT (Evans thermostat[51]) has been used. Data collections have been performed every 50 time steps during the last 15 000 of 35000 time steps using the microcanonical ensemble NVE.

Each glass structure obtained by the MD simulation has been analyzed in terms of radial distribution functions, bond angle distribution function, and ring size distributions using an algorithm developed by Yuan and Cormack.[52] The short-range order has been compared with the results of neutron diffraction[53-55] and extended X-ray absorption fine structure (EXAFS) studies.[56-58]

Mechanical properties ($E$, $G$, $B$, $\nu$) have also been calculated for each final configuration by means of the GULP code.[36] Space group $P1$ has been used to simulate a cubic cell with no symmetry. As a consequence, non-isotropic results, with slightly different values according to the direction chosen, have been obtained. However, since the differences are small, the Young's modulus for the glass has been calculated as the average of the three principal values.

## 3. Results and Discussion

**3.1. Binary Oxides.** The potential parameters of the Morse form of eq 4 are listed in Table 2; all potentials have been derived using the relaxed fitting combined with Gibbs free energy minimization at $T = 300$ K and $P = 1$ atm, as outlined above. Structural parameters for the oxides have been obtained from the Inorganic Crystal Structure Database,[59] while the elastic constants have been obtained from ref 47. Table 3 lists the conventional cell structural parameters that are calculated with the newly derived potentials for binary oxides. Typical estimated errors of the computed structural parameters (lattice vectors, cation–oxygen distances, and cell volume) are well below 1%. Higher errors have been encountered in the elastic constant calculations; however, in this case, typical errors of 10−15% may be considered good results. In fact, experimental elastic constant measurements strictly depend on the history and the number of defects of the sample under investigation, and measures carried out in different laboratories show significant different values. As an example, we mention the case of zircon $Zr_2SiO_4$ in which $C_{11}$ and $C_{12}$ elastic constants reported in ref 60 are 423.7 and 70.3 GPa, while the values from ref 61 are 258.5 and 179.1 GPa, respectively. It is noteworthy that the overall agreement is as good as can be expected for rocksalt structured oxides because of the validity of the Cauchy relation[62] ($C_{12} = C_{44}$) since central force potentials are used.

**3.2. Silicate Crystals.** The potentials developed have been applied to the prediction of structures and mechanical properties of a range of silicate minerals by means of the free energy minimization technique at $T = 300$ K and $P = 1$ atm.

The results obtained are discussed in the following for structural subclasses: nesosilicates (single tetrahedrons), sorosilicates (double tetrahedrons), inosilicates (single and double chains), cyclosilicates (rings), phyllosilicates (sheets), and tectosilicates (frameworks).

The experimental structures have been used as initial models, then the free energy has been minimized, and the final structures

**TABLE 2: Potential Parameters of Eq 4 Derived from Binary Oxides[a]**

| | $D_{ij}$ (eV) | $a_{ij}$ ($\text{Å}^{-2}$) | $r_0$ (Å) | $C_{ij}$ (eV $\text{Å}^{12}$) |
|---|---|---|---|---|
| $Li^{0.6}-O^{-1.2}$ | 0.001114 | 3.429506 | 2.681360 | 1.0 |
| $Na^{0.6}-O^{-1.2}$ | 0.023363 | 1.763867 | 3.006315 | 5.0 |
| $K^{0.6}-O^{-1.2}$ | 0.011612 | 2.062605 | 3.305308 | 5.0 |
| $Be^{1.2}-O^{-1.2}$ | 0.239919 | 2.527420 | 1.815405 | 1.0 |
| $Mg^{1.2}-O^{-1.2}$ | 0.038908 | 2.281000 | 2.586153 | 5.0 |
| $Ca^{1.2}-O^{-1.2}$ | 0.030211 | 2.241334 | 2.923245 | 5.0 |
| $Sr^{1.2}-O^{-1.2}$ | 0.019623 | 1.886000 | 3.328330 | 3.0 |
| $Ba^{1.2}-O^{-1.2}$ | 0.065011 | 1.547596 | 3.393410 | 5.0 |
| $Sc^{1.8}-O^{-1.2}$ | 0.000333 | 3.144445 | 3.200000 | 2.6 |
| $Ti^{2.4}-O^{-1.2}$ | 0.024235 | 2.254703 | 2.708943 | 1.0 |
| $Zr^{2.4}-O^{-1.2}$ | 0.206237 | 2.479675 | 2.436997 | 1.0 |
| $Cr^{1.8}-O^{-1.2}$ | 0.399561 | 1.785079 | 2.340810 | 1.0 |
| $Mn^{1.2}-O^{-1.2}$ | 0.029658 | 1.997543 | 2.852075 | 3.0 |
| $Fe^{1.2}-O^{-1.2}$ | 0.078171 | 1.822638 | 2.658163 | 2.0 |
| $Fe^{1.8}-O^{-1.2}$ | 0.418981 | 1.620376 | 2.382183 | 2.0 |
| $Co^{1.2}-O^{-1.2}$ | 0.012958 | 2.361272 | 2.756282 | 3.0 |
| $Ni^{1.2}-O^{-1.2}$ | 0.029356 | 2.679137 | 2.500754 | 3.0 |
| $Cu^{0.6}-O^{-1.2}$ | 0.090720 | 3.802168 | 2.055405 | 1.0 |
| $Ag^{0.6}-O^{-1.2}$ | 0.088423 | 3.439162 | 2.265956 | 1.0 |
| $Zn^{1.2}-O^{-1.2}$ | 0.001221 | 3.150679 | 2.851850 | 1.0 |
| $Al^{1.8}-O^{-1.2}$ | 0.361581 | 1.900442 | 2.164818 | 0.9 |
| $Si^{2.4}-O^{-1.2}$ | 0.340554 | 2.006700 | 2.100000 | 1.0 |
| $Ge^{2.4}-O^{-1.2}$ | 0.158118 | 2.294230 | 2.261313 | 5.0 |
| $Sn^{2.4}-O^{-1.2}$ | 0.079400 | 2.156770 | 2.633076 | 3.0 |
| $P^{3.0}-O^{-1.2}$ | 0.831326 | 2.585833 | 1.800790 | 1.0 |
| $Nd^{1.8}-O^{-1.2}$ | 0.014580 | 1.825100 | 3.398717 | 3.0 |
| $Gd^{1.8}-O^{-1.2}$ | 0.000132 | 2.013000 | 4.351589 | 3.0 |
| $Er^{1.8}-O^{-1.2}$ | 0.040448 | 2.294078 | 2.837722 | 3.0 |
| $O^{-1.2}-O^{-1.2}$ | 0.042395 | 1.379316 | 3.618701 | 22.0[b] |

[a] Li–O, Na–O, and K–O interatomic potential parameters were derived from silicates of the formula $M_2Si_2O_5$. The cutoff of the short-range interactions was set to 15 Å (see text for details). [b] The term $D/r^{12}$ is needed only in MD simulations and in free energy calculation at high temperature and pressure. In fact, the $D_{OO}$ term can range between 22 and 100 eV $\text{Å}^{12}$ without altering the results of free energy minimization at room temperature.

and the elastic constants have been compared with the experimental ones available in the literature.[63]

The structures investigated are listed in Tables 4−11, where they have been classified according to the nature of the silicate subclasses.

*3.2.1. Nesosilicates.* This subclass includes all silicates where the [SiO$_4$] tetrahedrons are isolated. Several types of silicate minerals are considered here, namely, the olivine, garnet, phenacite, zircon, and sillimanite and andalusite groups.

3.2.1.1. Olivine. The olivine structure of general formula $M_2SiO_4$ is based on a hexagonally close-packed oxygen sublattice with an orthorhombic unit cell. The structure has six sites: three for the oxygen, one tetrahedral site for the silicon, and two octahedral sites occupied by divalent cations. We have considered six compounds, namely, $Mg_2SiO_4$ (forsterite), $Fe_2SiO_4$ (fayalite), $Mn_2SiO_4$ (tephoroite), $CaMgSiO_4$ (monticellite), $Ni_2SiO_4$, and $Co_2SiO_4$. After free energy minimization at ambient conditions, the lattice vectors are reproduced with a typical error <2%, and the major errors have to be attributed to the average Si−O distance, which is about 2% smaller than the experimental one. This is due to the fact that the Si−O interaction has been fitted on α-quartz, which is a tectosilicate containing only bridging oxygen atoms. To overcome this problem one could assign, when modeling crystal structures, different short-range interactions to nonbridging oxygen (NBO) and bridging oxygen (BO), which are located at different positions in the unit cell. However, in melt materials the oxygen is able to diffuse in the bulk, and it can easily change its status from NBO to BO or vice versa. It would be necessary, therefore, to use a charge-

**TABLE 3: Structural Parameters for Fitted Binary Oxides**

| oxide | | a (Å) | b (Å) | c (Å) | α (deg) | β (deg) | γ (deg) | $V_{cell}$ (Å³) | <M−O> | $C_{11}$ | $C_{22}$ | $C_{33}$ | $C_{44}$ | $C_{55}$ | $C_{66}$ | $C_{12}$ | $C_{13}$ | $C_{14}$ | $C_{23}$ | B |
|---|---|---|---|---|---|---|---|---|---|---|---|---|---|---|---|---|---|---|---|---|
| $Cu_2O$ | expt | 4.2696 | 4.2696 | 4.2696 | 90 | 90 | 90 | 77.833 | 1.8488 | 11.60 | | | 1.10 | | | 10.50 | | | | 11.20 |
| cuprite | calcd | 4.2704 | 4.2704 | 4.2704 | 90 | 90 | 90 | 77.875 | 1.8491 | 10.58 | | | 1.94 | | | 11.38 | | | | 11.12 |
| | % error | 0.02 | 0.02 | 0.02 | 0 | 0 | 0 | 0.05 | 0.02 | −8.80 | | | 79 | | | 8.38 | | | | −0.71 |
| $Ag_2O$ | expt | 4.7200 | 4.7200 | 4.7200 | 90 | 90 | 90 | 105.154 | 2.0438 | | | | | | | | | | | |
| | calcd | 4.7200 | 4.7200 | 4.7200 | 90 | 90 | 90 | 105.154 | 2.0438 | | | | | | | | | | | |
| | % error | 0.00 | 0.00 | 0.00 | 0 | 0 | 0 | 0.00 | 0.00 | | | | | | | | | | | |
| BeO | expt | 2.6750 | 2.6750 | 4.3410 | 90 | 90 | 120 | 26.901 | 1.6347 | 47.0 | | 49.4 | 15.30 | | | 16.8 | 11.9 | | | 25.1 |
| bromellite | calcd | 2.6984 | 2.6984 | 4.3349 | 90 | 90 | 120 | 27.336 | 1.6439 | 47.58 | | 48.1 | 14.39 | | | 17.87 | 14.39 | | | 26.27 |
| | % error | 0.87 | 0.87 | −0.14 | 0 | 0 | 0 | 1.62 | 0.56 | 1.2 | | −2.6 | −5.9 | | | 6.4 | 20.9 | | | 1.62 |
| ZnO | expt | 3.2494 | 3.2494 | 5.2038 | 90 | 90 | 120 | 47.584 | 1.9775 | 20.90 | | 21.80 | 4.41 | | | 12.00 | 10.4 | | | 14.35 |
| zincite | calcd | 3.2463 | 3.2463 | 5.0974 | 90 | 90 | 120 | 46.522 | 1.9637 | 21.29 | | 17.77 | 4.31 | | | 13.99 | 12.1 | | | 14.90 |
| | % error | −0.1 | −0.1 | −2.0 | 0 | 0 | 0 | −2.2 | −0.7 | 1.87 | | −18.5 | −2.2 | | | 16.6 | 16.3 | | | 3.8 |
| MgO | expt | 4.2170 | 4.2170 | 4.2170 | 90 | 90 | 90 | 74.991 | 2.1086 | 29.40 | | | 15.5 | | | 9.30 | | | | 16.0 |
| periclase | calcd | 4.2394 | 4.2394 | 4.2394 | 90 | 90 | 90 | 76.192 | 2.1197 | 29.46 | | | 10.53 | | | 10.53 | | | | 16.84 |
| | % error | 0.53 | 0.53 | 0.53 | 0 | 0 | 0 | 1.60 | 0.53 | 0.20 | | | −32 | | | 13 | | | | 5.3 |
| CaO | expt | 4.8105 | 4.8105 | 4.8105 | 90 | 90 | 90 | 111.319 | 2.4052 | 22.40 | | | 8.06 | | | 6.00 | | | | 11.47 |
| lime | calcd | 4.7748 | 4.7748 | 4.7748 | 90 | 90 | 90 | 108.861 | 2.3874 | 26.87 | | | 4.56 | | | 4.56 | | | | 11.96 |
| | % error | −0.74 | −0.74 | −0.74 | 0 | 0 | 0 | −2.2 | −0.74 | 20 | | | 43 | | | 24 | | | | 4.27 |
| SrO | expt | 5.1500 | 5.1500 | 5.1500 | 90 | 90 | 90 | 136.591 | 2.5750 | 17.00 | | | 5.56 | | | 4.6 | | | | 8.73 |
| | calcd | 5.1453 | 5.1453 | 5.1453 | 90 | 90 | 90 | 136.213 | 2.5726 | 17.13 | | | 2.84 | | | 2.84 | | | | 7.60 |
| | % error | −0.09 | −0.09 | −0.09 | 0 | 0 | 0 | −0.28 | −0.09 | 0.76 | | | −49 | | | −38 | | | | −12.9 |
| BaO | expt | 5.5300 | 5.5300 | 5.5300 | 90 | 90 | 90 | 169.112 | 2.765 | 12.2 | | | 3.44 | | | 4.5 | | | | 7.07 |
| | calcd | 5.5011 | 5.5011 | 5.5011 | 90 | 90 | 90 | 166.475 | 2.7505 | 13.78 | | | 1.71 | | | 1.71 | | | | 5.73 |
| | % error | −0.52 | −0.52 | −0.52 | 0 | 0 | 0 | −1.56 | −0.52 | 13.0 | | | −50 | | | −62 | | | | −19 |
| FeO | expt | 4.3000 | 4.3000 | 4.3000 | 90 | 90 | 90 | 79.507 | 2.1500 | 35.9 | | | 5.6 | | | 15.6 | | | | 22.37 |
| wustite | calcd | 4.2835 | 4.2835 | 4.2835 | 90 | 90 | 90 | 78.595 | 2.1417 | 32.45 | | | 9.77 | | | 9.77 | | | | 17.33 |
| | % error | −0.38 | −0.38 | −0.38 | 0 | 0 | 0 | −1.15 | −0.39 | −9.6 | | | 74 | | | −37 | | | | −22.5 |
| CoO | expt | 4.2500 | 4.2500 | 4.2500 | 90 | 90 | 90 | 76.766 | 2.1250 | 26.00 | | | 8.24 | | | 14.5 | | | | 18.33 |
| | calcd | 4.2425 | 4.2425 | 4.2425 | 90 | 90 | 90 | 76.361 | 2.1213 | 26.13 | | | 10.69 | | | 10.69 | | | | 15.84 |
| | % error | −0.18 | −0.18 | −0.18 | 0 | 0 | 0 | −0.53 | −0.17 | 0.5 | | | 30 | | | −26 | | | | −13.6 |
| NiO | expt | 4.1946 | 4.1946 | 4.1946 | 90 | 90 | 90 | 73.803 | 2.0973 | 34.46 | | | 4.0 | | | 14.1 | | | | 20.5 |
| bunsenite | calcd | 4.1890 | 4.1890 | 4.1890 | 90 | 90 | 90 | 73.507 | 2.0945 | 34.57 | | | 11.69 | | | 11.69 | | | | 19.32 |
| | % error | −0.13 | −0.13 | −0.13 | 0 | 0 | 0 | −0.4 | −0.13 | 0.32 | | | 192 | | | −17 | | | | −5.8 |
| MnO | expt | 4.4448 | 4.4448 | 4.4448 | 90 | 90 | 90 | 87.813 | 2.2224 | 22.70 | | | 7.80 | | | 11.60 | | | | 15.30 |
| manganosite | calcd | 4.4398 | 4.4398 | 4.4398 | 90 | 90 | 90 | 87.516 | 2.2199 | 23.66 | | | 7.48 | | | 7.48 | | | | 12.87 |
| | % error | −0.11 | −0.11 | −0.11 | 0 | 0 | 0 | −0.34 | −0.11 | 4.23 | | | −4.1 | | | −36 | | | | −15.9 |
| $Al_2O_3$ | expt | 4.7602 | 4.7602 | 12.9933 | 90 | 90 | 120 | 254.977 | 1.9134 | 49.70 | | 50.10 | 14.68 | | | 16.20 | 11.60 | −2.14 | | 25.35 |
| α-corundum | calcd | 4.7113 | 4.7113 | 13.0119 | 90 | 90 | 120 | 250.121 | 1.9072 | 48.82 | | 50.18 | 11.38 | | | 19.70 | 15.00 | −2.96 | | 27.45 |
| | % error | −1.03 | −1.03 | 0.14 | 0 | 0 | 0 | −1.9 | −0.32 | −1.77 | | 0.16 | −22.5 | | | 21.6 | 29.3 | 38.3 | | 8.3 |
| $Fe_2O_3$ | expt | 4.9666 | 4.9666 | 13.4251 | 90 | 90 | 120 | 286.792 | 2.0045 | | | | | | | | | | | 20.66 |
| hematite | calcd | 4.9524 | 4.9524 | 13.4237 | 90 | 90 | 120 | 285.121 | 1.9903 | | | | | | | | | | | 22.91 |
| | % error | −0.29 | −0.29 | −0.01 | 0 | 0 | 0 | −0.58 | −0.71 | | | | | | | | | | | 10.9 |
| $Cr_2O_3$ | expt | 4.9607 | 4.9607 | 13.5990 | 90 | 90 | 120 | 289.817 | 1.9906 | 37.40 | | 36.2 | 15.9 | | | 14.80 | 17.50 | | | 23.40 |
| eskolaite | calcd | 5.0017 | 5.0017 | 13.5945 | 90 | 90 | 120 | 294.529 | 2.0086 | 39.32 | | 35.31 | 12.82 | | | 16.89 | 17.5 | | | 23.73 |
| | % error | 0.83 | 0.83 | −0.03 | 0 | 0 | 0 | 1.63 | 0.90 | 5.13 | | −2.5 | −19.4 | | | 14.1 | 16.6 | | | 1.41 |
| $Sc_2O_3$ | expt | 9.8459 | 9.8459 | 9.8459 | 90 | 90 | 90 | 954.479 | 2.1304 | | | | | | | | | | | |
| | calcd | 9.8648 | 9.8648 | 9.8648 | 90 | 90 | 90 | 959.976 | 2.1249 | | | | | | | | | | | |
| | % error | 0.19 | 0.19 | 0.19 | 0 | 0 | 0 | 0.58 | −0.26 | | | | | | | | | | | |

lattice parameters — elastic constants ($10^{10}$ Pa)

**TABLE 3: (Continued)**

| oxide | | a (Å) | b (Å) | c (Å) | α (deg) | β (deg) | γ (deg) | $V_{cell}$ (Å³) | <M−O> | $C_{11}$ | $C_{22}$ | $C_{33}$ | $C_{44}$ | $C_{55}$ | $C_{66}$ | $C_{12}$ | $C_{13}$ | $C_{14}$ | $C_{23}$ | B |
|---|---|---|---|---|---|---|---|---|---|---|---|---|---|---|---|---|---|---|---|---|
| | | lattice parameters | | | | | | | | elastic constants ($10^{10}$ Pa) | | | | | | | | | | |
| Nd₂O₃ | expt | 11.0740 | 11.0740 | 11.0740 | 90 | 90 | 90 | 1358.04 | 2.3830 | | | | | | | | | | | |
| | calcd | 11.0693 | 11.0693 | 11.0693 | 90 | 90 | 90 | 1356.32 | 2.3847 | | | | | | | | | | | |
| | % error | −0.04 | −0.04 | −0.04 | 0 | 0 | 0 | −0.12 | 0.07 | | | | | | | | | | | |
| Gd₂O₃ | expt | 10.8090 | 10.8090 | 10.8090 | 90 | 90 | 90 | 1262.86 | 2.3264 | | | | | | | | | | | 11.58 |
| | calcd | 10.8047 | 10.8047 | 10.8047 | 90 | 90 | 90 | 1261.36 | 2.3282 | | | | | | | | | | | 10.07 |
| | % error | −0.04 | −0.04 | −0.04 | 0 | 0 | 0 | −0.11 | 0.08 | | | | | | | | | | | −13.0 |
| Er₂O₃ | expt | 10.5360 | 10.5360 | 10.5360 | 90 | 90 | 90 | 1169.57 | 2.2711 | | | | | | | | | | | 14.04 |
| | calcd | 10.5306 | 10.5306 | 10.5306 | 90 | 90 | 90 | 1167.79 | 2.2677 | | | | | | | | | | | 14.43 |
| | % error | −0.05 | −0.05 | −0.05 | 0 | 0 | 0 | −0.15 | −0.15 | | | | | | | | | | | 2.78 |
| SiO₂ | expt | 4.9160 | 4.9160 | 5.4054 | 90 | 90 | 120 | 113.13 | 1.609 | 8.66 | | 10.61 | 5.78 | | | 0.67 | 1.26 | −1.78 | | 3.78 |
| α-quartz | calcd | 4.9241 | 4.9241 | 5.4333 | 90 | 90 | 120 | 114.092 | 1.602 | 8.68 | | 10.63 | 4.95 | | | 0.88 | 1.18 | −1.78 | | 3.79 |
| | % error | 0.16 | 0.16 | 0.52 | 0 | 0 | 0 | 0.85 | −0.44 | 0.23 | | 0.19 | −14.4 | | | 31.3 | −6.4 | 0.0 | | 0.26 |
| GeO₂ | expt | 4.3930 | 4.3930 | 2.8626 | 90 | 90 | 90 | 55.244 | 1.8811 | 33.72 | | 59.94 | 16.15 | | 25.84 | 18.82 | 18.74 | | | 25.76 |
| | calcd | 4.4261 | 4.4261 | 2.8798 | 90 | 90 | 90 | 56.417 | 1.8961 | 43.50 | | 57.65 | 16.89 | | 19.51 | 18.39 | 18.43 | | | 27.92 |
| | % error | 0.68 | 0.68 | 0.60 | 0 | 0 | 0 | 2.1 | 0.80 | 29.0 | | −3.82 | 4.58 | | −24.5 | −2.28 | −1.65 | | | 8.39 |
| TiO₂ | expt | 4.5930 | 4.5930 | 2.9590 | 90 | 90 | 90 | 62.422 | 1.9587 | 26.9 | | 48.0 | 12.4 | | 19.20 | 17.7 | 14.60 | | | 21.55 |
| rutile | calcd | 4.5718 | 4.5718 | 3.0046 | 90 | 90 | 90 | 62.799 | 1.9663 | 34.78 | | 45.64 | 13.48 | | 16.64 | 16.0 | 14.48 | | | 22.56 |
| | % error | −0.46 | −0.46 | 1.54 | 0 | 0 | 0 | 0.60 | 0.4 | 29.3 | | −4.9 | 8.71 | | −13.3 | −9.5 | −0.82 | | | 4.7 |
| SnO₂ | expt | 4.7373 | 4.7373 | 3.1864 | 90 | 90 | 90 | 71.509 | 2.0535 | 26.17 | | 44.96 | 10.31 | | 20.74 | 17.72 | 15.55 | | | 21.23 |
| cassiterite | calcd | 4.7599 | 4.7599 | 3.1684 | 90 | 90 | 90 | 71.786 | 2.0572 | 30.21 | | 42.14 | 12.55 | | 18.47 | 18.79 | 13.13 | | | 21.30 |
| | % error | 0.48 | 0.48 | −0.56 | 0 | 0 | 0 | 0.39 | 0.18 | 15.44 | | −6.3 | 21.73 | | −10.9 | 6.0 | −15.6 | | | 0.33 |
| ZrO₂ | expt | 5.1690 | 5.2320 | 5.3410 | 90 | 99.25 | 90 | 142.565 | 2.1661 | | | | | | | | | | | |
| | calcd | 5.2074 | 5.2135 | 5.2796 | 90 | 99.03 | 90 | 141.558 | 2.1647 | | | | | | | | | | | |
| | % error | 0.74 | −0.35 | −1.15 | 0 | −0.22 | 0 | −0.71 | −0.06 | | | | | | | | | | | |
| P₄O₁₀ | expt | 9.8257 | 9.8257 | 13.6455 | 90 | 90 | 120 | 1140.89 | 1.558 | | | | | | | | | | | |
| | calcd | 9.8298 | 9.8298 | 13.6315 | 90 | 90 | 120 | 1140.67 | 1.5454 | | | | | | | | | | | |
| | % error | 0.04 | 0.04 | −0.1 | 0 | 0 | 0 | −0.02 | −0.8 | | | | | | | | | | | |
| | % error | −0.04 | −0.04 | −0.04 | 0 | 0 | 0 | −0.12 | 0.07 | | | | | | | | | | | |

**TABLE 4: Structural and Mechanical Properties for Selected Crystal Silicates (Olevine)**

| | | lattice parameters | | | | | | | | elastic constants ($10^{10}$ Pa) | | | | | | | | | | |
|---|---|---|---|---|---|---|---|---|---|---|---|---|---|---|---|---|---|---|---|---|---|
| | | $a$ (Å) | $b$ (Å) | $c$ (Å) | $\alpha$ (deg) | $V_{cell}$ (Å³) | <Si−O> | <M−O> | <MI−O> | $C_{11}$ | $C_{22}$ | $C_{33}$ | $C_{44}$ | $C_{55}$ | $C_{66}$ | $C_{12}$ | $C_{13}$ | $C_{14}$ | $C_{23}$ | $B$ |
| Mg$_2$SiO$_4$ forsterite | expt | 4.7530 | 10.1900 | 5.9780 | 90 | 289.5329 | 1.6352 | 2.1117 | | 32.8 | 20.0 | 23.5 | 6.67 | 8.13 | 8.09 | 6.9 | 6.9 | | 7.3 | 12.95 |
| | calcd | 4.8447 | 10.1875 | 6.0022 | 90 | 296.2444 | 1.6022 | 2.1126 | | 29.82 | 17.46 | 21.6 | 3.87 | 5.85 | 6.82 | 6.94 | 7.41 | | 7.44 | 11.99 |
| | % error | 1.9 | −0.02 | 0.4 | 0 | 2.3 | −2.0 | 0.04 | | 9.1 | −12.7 | −8.0 | −42.0 | −28.0 | −15.7 | 0.6 | 7.4 | | 1.9 | −7.41 |
| Fe$_2$SiO$_4$ fayalite | expt | 4.8200 | 10.4790 | 6.0870 | 90 | 307.4469 | 1.6366 | 2.1649 | | 26.6 | 16.8 | 23.2 | 3.23 | 4.65 | 5.70 | 9.40 | 9.20 | | 9.20 | 13.4 |
| | calcd | 4.8727 | 10.2539 | 6.0564 | 90 | 302.6050 | 1.6024 | 2.1623 | | 29.6 | 17.85 | 21.74 | 5.06 | 6.43 | 7.20 | 7.68 | 8.16 | | 7.60 | 12.37 |
| | % error | 1.1 | −2.1 | −0.5 | 0 | −1.6 | −2.1 | −0.1 | | 11.3 | 6.3 | −6.3 | 56.7 | 38 | 26.3 | −18.3 | −11.3 | | −17.4 | −7.7 |
| Mn$_2$SiO$_4$ tephroite | expt | 4.9020 | 10.5960 | 6.2570 | 90 | 324.999 | 1.6387 | 2.2129 | | 25.84 | 16.56 | 20.68 | 4.53 | 5.56 | 5.78 | 8.70 | 9.50 | | 9.20 | 12.8 |
| | calcd | 4.9834 | 10.5477 | 6.2537 | 90 | 328.717 | 1.6028 | 2.2390 | | 22.79 | 13.29 | 17.16 | 3.94 | 5.25 | 5.80 | 6.08 | 6.43 | | 5.99 | 9.56 |
| | % error | 1.66 | −0.46 | −0.05 | 0 | 1.14 | −2.2 | 1.17 | | −11.8 | −19.8 | −17.0 | −13.0 | −5.6 | 0.3 | −30.1 | −32.3 | | −35 | −25.3 |
| CaMgSiO$_4$ monticellite | expt | 4.8220 | 11.1080 | 6.3820 | 90 | 341.838 | 1.6262 | 2.3703 | 2.1327 | 21.6 | 15.0 | 18.4 | 5.06 | 5.65 | 5.92 | 5.90 | 7.10 | | 7.70 | 10.6 |
| | calcd | 4.8982 | 11.0653 | 6.3872 | 90 | 346.189 | 1.5992 | 2.3853 | 2.1353 | 21.24 | 13.58 | 17.56 | 4.26 | 5.36 | 5.63 | 6.56 | 7.55 | | 7.2 | 10.19 |
| | % error | 1.58 | −0.38 | 0.08 | 0 | 1.27 | −1.66 | 0.63 | 0.12 | −1.67 | −9.47 | −4.57 | −15.8 | −5.1 | −4.9 | 11.2 | 6.3 | | −6.5 | −3.9 |
| Ni$_2$SiO$_4$ | expt | 4.7296 | 10.1209 | 5.9150 | 90 | 283.138 | 1.6396 | 2.0871 | | 34.0 | 23.80 | 25.30 | 7.10 | 8.70 | 7.80 | 10.90 | 11.00 | | 11.3 | 16.5 |
| | calcd | 4.8070 | 10.0909 | 5.9407 | 90 | 288.164 | 1.6026 | 2.119 | | 33.06 | 19.75 | 23.82 | 4.07 | 6.41 | 7.51 | 7.74 | 8.29 | | 8.16 | 13.35 |
| | % error | 1.6 | −0.3 | 0.4 | 0 | 1.8 | −2.3 | 1.5 | | −2.8 | −17.0 | −5.8 | −42.7 | −26 | −3.7 | −29 | −24.6 | | −28 | −19 |
| Co$_2$SiO$_4$ | expt | 4.7820 | 10.3020 | 6.0030 | 90 | 295.733 | 1.6265 | 2.1305 | | 30.78 | 19.47 | 23.42 | 4.67 | 6.39 | 6.48 | 10.2 | 10.5 | | 10.3 | 14.8 |
| | calcd | 4.8483 | 10.2194 | 6.0025 | 90 | 297.404 | 1.6033 | 2.1481 | | 28.6 | 16.15 | 20.8 | 2.04 | 5.20 | 6.22 | 6.05 | 6.66 | | 7.03 | 11.16 |
| | % error | 1.38 | −0.8 | 0.01 | 0 | 0.6 | −1.4 | 0.8 | | −7.1 | −17.1 | −11.2 | −56.3 | −19 | −4.0 | −40.7 | −36.6 | | −32 | −24.6 |

variable potential model, but this choice would be very computationally expensive.

Bulk moduli for forsterite, fayalite, and monticellite are predicted with an error less than 10%, while for the other structures the bulk moduli are estimated within an error of about 20%. The typical errors for the elastic constants are of the same order of magnitude.

3.2.1.2 Garnets. The general formula for most of the garnets is A$_3$B$_2$(SiO$_4$)$_3$, where A represents a divalent metal such as calcium, iron, magnesium, or manganese placed in dodecahedral sites and B represents a trivalent metal such as aluminum, chromium, or iron placed in octahedral sites. Garnets are isostructural, meaning that they share the same crystal structure and belong to the isometric crystal class, which produces very symmetrical, cube-based crystals. We have considered four compounds, namely, Mg$_3$Al$_2$Si$_3$O$_{12}$ (pyrope), Ca$_3$Al$_2$Si$_3$O$_{12}$ (grossular), Mn$_3$Al$_2$Si$_3$O$_{12}$ (spessartite), and Ca$_3$Fe$_2$Si$_3$O$_{12}$ (andradite). Despite an error of about 2% for the Si−O average distance, the lattice vectors show a typical error less than 0.7%. The errors for the average distances of the divalent and trivalent cations with the oxygen are about 1.5%. A very good agreement is found for mechanical properties that have a typical error below 10% for all the crystals considered.

3.2.1.3. Phenacite. This class of mineral includes phenacite itself (Be$_2$SiO$_4$) and willemite (Zn$_2$SiO$_4$). Both the divalent cations and the silicon ions occupy tetrahedral sites. Results show that both the minerals are well reproduced, and in fact, typical errors are less than 0.5% for lattice parameters and the average divalent cation oxygen distances. The average Si−O distances are predicted with an error within 1.5%. Good agreement has been found with regards to the prediction of mechanical properties of phenacite, with errors below 10%. To our knowledge, no data are available for mechanical properties of willemite in the literature.

3.2.1.4. Zircon. The zircon structure also contains isolated silicate tetrahedra with zirconium 8-fold coordinated by the oxygen sublattice. The structure is tetragonal with the zirconium and silicon ions occupying special sites. In this case the structure is reproduced with errors below 1.7% while higher errors have been obtained in the calculation of mechanical properties such as $C_{11}$ and $C_{12}$ elastic constants.

3.2.1.5. Andalusite and Sillimanite. Typical errors of about 2% are found in lattice vectors and Si−O distances; however, it is noteworthy that the Al−O potential parameters that we have fitted for the octahedral sites in α-corundum are able to reproduce both the distances and the sites of the pentacoordinated and tetracoordinated Al cations in andalusite and sillimanite, respectively. Bulk moduli are predicted with an error of 5%, and most of the elastic constants are calculated with an error less than 10%.

*3.2.2. Sorosilicates.* Sorosilicates contain units made up of two tetrahedra that share one oxygen; the basic chemical unit is the anionic group [Si$_2$O$_7$]$^{6-}$. This structure forms an unusual hourglass-like shape. We have considered here the thortveitite mineral (Sc$_2$Si$_2$O$_7$, which features octahedral sites for Sc$^{III}$ and a linear Si−O−Si bond between staggered tetrahedra), barylite (BaBe$_2$Si$_2$O$_7$), and hardystonite (Ca$_2$ZnSi$_2$O$_7$). The typical errors in the Si−O average distances are about 1.5%. An error of 2.8% is found for the *c*-axis in thortveitite, while for the other structures the cell parameters are predicted with errors less than 1.5%. The computed cell volume in hardystonite is greater than the experimental one because of the larger Ca−O distances (error 2.8%). Experimental mechanical properties are not available.

**TABLE 5: Structural and Mechanical Properties for Selected Crystal Silicates (Garnets)**

| | | lattice parameters | | | | | | | | elastic constants ($10^{10}$ Pa) | | | | | | | | | | |
|---|---|---|---|---|---|---|---|---|---|---|---|---|---|---|---|---|---|---|---|---|
| | | $a$ (Å) | $b$ (Å) | $c$ (Å) | $\alpha$ (deg) | $V_{cell}$ (Å$^3$) | <Si–O> | <Al/Fe–O> | <M–O> | $C_{11}$ | $C_{22}$ | $C_{33}$ | $C_{44}$ | $C_{55}$ | $C_{66}$ | $C_{12}$ | $C_{13}$ | $C_{14}$ | $C_{23}$ | $B$ |
| Mg$_3$Al$_2$Si$_3$O$_{12}$ | expt | 11.5480 | 11.5480 | 11.5480 | 90 | 1539.999 | 1.6361 | 1.8966 | 2.3007 | 29.62 | | | 9.00 | | | 11.11 | | | | 17.28 |
| pyrope | calcd | 11.5515 | 11.5515 | 11.5515 | 90 | 1541.423 | 1.5942 | 1.9215 | 2.3195 | 26.68 | | | 8.57 | | | 11.76 | | | | 16.73 |
| | % error | 0.03 | 0.03 | 0.03 | 0 | 0.09 | −2.6 | 1.3 | 0.8 | −9.9 | | | −4.8 | | | 5.9 | | | | −3.2 |
| Ca$_3$Al$_2$Si$_3$O$_{12}$ | expt | 11.8370 | 11.8370 | 11.8370 | 90 | 1658.536 | 1.6460 | 1.9237 | 2.4020 | 32.17 | | | 10.46 | | | 9.12 | | | | 16.84 |
| grossular | calcd | 11.9182 | 11.9182 | 11.9182 | 90 | 1692.918 | 1.6105 | 1.9663 | 2.4383 | 29.16 | | | 9.53 | | | 10.5 | | | | 16.72 |
| | % error | 0.7 | 0.7 | 0.7 | 0 | 2.1 | 2.1 | 2.2 | 1.5 | −9.4 | | | −8.9 | | | 15.1 | | | | −0.7 |
| Mn$_3$Al$_2$Si$_3$O$_{12}$ | expt | 11.6190 | 11.6190 | 11.6190 | 90 | 1568.579 | 1.6398 | 1.9010 | 2.3252 | 30.95 | | | 9.52 | | | 11.35 | | | | 17.88 |
| spessartite | calcd | 11.6935 | 11.6935 | 11.6935 | 90 | 1598.933 | 1.6003 | 1.9372 | 2.3654 | 26.92 | | | 9.52 | | | 10.78 | | | | 16.16 |
| | % error | 0.6 | 0.6 | 0.6 | 0 | 1.94 | −2.4 | 1.9 | 1.7 | −13.0 | | | 0.0 | | | −5.0 | | | | −9.6 |
| Ca$_3$Fe$_2$Si$_3$O$_{12}$ | expt | 12.0310 | 12.0310 | 12.0310 | 90 | 1741.427 | 1.6409 | 2.0187 | 2.4252 | 28.9 | | | 8.5 | | | 9.2 | | | | 15.7 |
| andradite | calcd | 12.0665 | 12.0665 | 12.0665 | 90 | 1756.900 | 1.6039 | 2.0463 | 2.4539 | 28.02 | | | 8.0 | | | 9.19 | | | | 15.47 |
| | % error | 0.3 | 0.3 | 0.3 | 0 | 0.9 | −2.2 | 1.4 | 1.2 | −3.0 | | | −5.6 | | | −0.1 | | | | −1.5 |

**TABLE 6: Structural and Mechanical Properties for Selected Crystal Silicates (Other Important Nesosilicates)**

| | | lattice parameters | | | | | | | | | elastic constants ($10^{10}$ Pa) | | | | | | | | | | |
|---|---|---|---|---|---|---|---|---|---|---|---|---|---|---|---|---|---|---|---|---|---|
| | | $a$ (Å) | $b$ (Å) | $c$ (Å) | $\alpha$ (deg) | $\beta$ (deg) | $\gamma$ (deg) | $V_{cell}$ (Å$^3$) | <Si–O> | <M–O> | $C_{11}$ | $C_{22}$ | $C_{33}$ | $C_{44}$ | $C_{55}$ | $C_{66}$ | $C_{12}$ | $C_{13}$ | $C_{14}$ | $C_{23}$ | $B$ |
| Be$_2$SiO$_4$ | expt | 12.4720 | 12.4720 | 8.2510 | 90 | 90 | 120 | 1111.494 | 1.6323 | 1.6444 | 34.19 | | 39.1 | 9.14 | | | 14.8 | 13.6 | 0.01 | | 21.28 |
| phenacite | calcd | 12.4180 | 12.4180 | 8.2533 | 90 | 90 | 120 | 1102.208 | 1.6079 | 1.6504 | 34.92 | | 38.35 | 9.64 | | | 14.63 | 12.34 | 0.05 | | 20.75 |
| | % error | −0.4 | −0.4 | −0.4 | 0 | 0 | 0 | −0.8 | −1.5 | 0.4 | 2.1 | | −1.9 | 5.5 | | | −1.1 | −9.2 | 400 | | −2.5 |
| Zn$_2$SiO$_4$ | expt | 13.9480 | 13.9480 | 9.3150 | 90 | 90 | 120 | 1569.413 | 1.6346 | 1.9553 | | | | | | | | | | | |
| willemite | calcd | 13.9012 | 13.9012 | 9.3093 | 90 | 90 | 120 | 1557.943 | 1.6082 | 1.9639 | | | | | | | | | | | |
| | % error | −0.3 | −0.3 | −0.06 | 0 | 0 | 0 | −0.7 | −1.6 | 0.4 | | | | | | | | | | | |
| ZrSiO$_4$ | expt | 6.6070 | 6.6070 | 5.9820 | 90 | 90 | 90 | 261.129 | 1.6223 | 2.1996 | 42.37 | | 49.0 | 11.36 | | | 7.03 | 14.95 | | | |
| zircon | calcd | 6.5654 | 6.5654 | 6.0777 | 90 | 90 | 90 | 261.979 | 1.5940 | 2.2358 | 52.74 | | 46.0 | 10.19 | | | 11.31 | 13.75 | | | 25.42 |
| | % error | −0.6 | −0.6 | 1.6 | 0 | 0 | 0 | 0.3 | −1.7 | 1.6 | 24.5 | | −6.1 | −10.3 | | | 61 | −8.0 | | | |
| Al$_2$SiO$_5$ | expt | 7.7942 | 7.8985 | 5.5590 | 90 | 90 | 90 | 342.226 | 1.6273 | 1.8834 | 23.34 | 28.9 | 38.01 | 9.95 | 8.78 | 11.23 | 9.77 | 11.62 | | 8.14 | 16.20 |
| andalusite | calcd | 7.6678 | 7.9595 | 5.5203 | 90 | 90 | 90 | 336.920 | 1.5967 | 1.8927 | 20.0 | 25.0 | 35.4 | 8.97 | 6.67 | 12.26 | 10.27 | 12.05 | | 10.9 | 15.4 |
| | % error | −1.6 | 0.8 | −0.7 | 0 | 0 | 0 | −1.5 | −1.9 | 0.5 | −14.0 | −13.6 | −6.9 | −9.8 | −24 | 9.2 | 5.1 | 3.7 | | 34 | −5 |
| Al$_2$SiO$_5$ | expt | 7.4856 | 7.6738 | 5.7698 | 90 | 90 | 90 | 331.435 | 1.6118 | 1.8526 | 28.73 | 23.19 | 38.84 | 12.24 | 8.07 | 8.93 | 15.86 | 8.3 | | 9.47 | 17.1 |
| sillimanite | calcd | 7.4001 | 7.4492 | 5.8238 | 90 | 90 | 90 | 321.037 | 1.5941 | 1.8487 | 30.04 | 25.16 | 39.87 | 12.26 | 7.77 | 8.35 | 10.22 | 11.44 | | 16.48 | 18.07 |
| | % error | −1.1 | −2.9 | 0.9 | 0 | 0 | 0 | 3.1 | −1.1 | −0.2 | 4.6 | 8.5 | 2.7 | 0.2 | −3.7 | −6.5 | −35.6 | 37.8 | | 74 | 5.8 |

**TABLE 7: Structural and Mechanical Properties for Selected Crystal Silicates (Sorosilicates)**

| | | | | lattice parameters | | | | | | | elastic constants ($10^{10}$ Pa) | | | | | | | | | | | |
|---|---|---|---|---|---|---|---|---|---|---|---|---|---|---|---|---|---|---|---|---|---|---|
| | | $a$ (Å) | $b$ (Å) | $c$ (Å) | $\beta$ (deg) | $V_{cell}$ (Å³) | <Si-O> | <M-O> | <MI-O> | $C_{11}$ | $C_{22}$ | $C_{33}$ | $C_{44}$ | $C_{55}$ | $C_{66}$ | $C_{12}$ | $C_{13}$ | $C_{14}$ | $C_{23}$ | $B$ |
| Ca₂ZnSi₂O₇ hardystonite | expt | 7.8280 | 7.8280 | 5.0140 | 90 | 307.246 | 1.6213 | 2.5687 | 1.9372 | | | | | | | | | | | |
| | calcd | 7.9470 | 7.9470 | 4.9981 | 90 | 315.658 | 1.5975 | 2.6315 | 1.9196 | | | | | | | | | | | |
| | % error | 1.5 | 1.5 | -0.3 | 0 | 2.7 | 1.5 | 2.4 | -0.9 | | | | | | | | | | | |
| Sc₂Si₂O₇ thortveitite | expt | 6.5030 | 8.4980 | 4.6820 | 102.77 | 252.339 | 1.6204 | 2.1217 | | | | | | | | | | | | |
| | calcd | 6.4429 | 8.4642 | 4.8141 | 102.78 | 256.026 | 1.6066 | 2.1461 | | | | | | | | | | | | |
| | % error | -0.9 | -0.4 | 2.8 | 0.01 | 1.46 | -0.85 | 1.15 | | | | | | | | | | | | |
| BaBe₂Si₂O₇ barylite | expt | 9.8200 | 11.6700 | 4.6900 | 90 | 537.471 | 1.6316 | 2.9787 | 1.6456 | | | | | | | | | | | |
| | calcd | 9.8738 | 11.7384 | 4.6178 | 90 | 535.217 | 1.6040 | 3.0102 | 1.6375 | | | | | | | | | | | |
| | % error | 0.5 | 0.6 | 1.5 | 0 | -0.4 | -1.7 | 1.1 | -0.5 | | | | | | | | | | | |

*3.2.3. Cyclosilicates.* Cyclic metasilicates $[(SiO_3)_n]^{2n-}$ having 3, 4, 6, or 8 linked tetrahedra are known, 3 and 6 being the most common values. We have studied two three-membered ring silicates, namely, $Na_2Be_2Si_3O_9$ and $BaTi(SiO_3)_3$ (benitoite) and one six-membered ring silicate, $Al_2Be_3Si_6O_{18}$ (beryl). The $Na_2Be_2Si_3O_9$ structure is orthorhombic with $Si_3O_9$ rings parallel to the (010) direction. These rings are linked by $Be_2O_6$ groups, which comprise two $BeO_4$ tetrahedra sharing one edge. Sodium is heptacoordinated. The structure is well reproduced with typical errors within 1%. Larger errors are found in the benitoite structure where lattice parameters are 1% larger and the cell volume is expanded by 3.5%. The reason might be due to the fact that the Ba—O distances are too long (4.3%). Both structural parameters and mechanical properties are well predicted with typical errors within 1% and less than 10% for beryl, respectively.

*3.2.4. Inosilicates.* Chain metasilicates $[SiO_3^{2-}]_\infty$ formed by corner sharing of $[SiO_4]$ tetrahedra are particularly prevalent in many important minerals. Despite the apparent simplicity of the structural motif and stoichiometry, many different structures are encountered because of the different conformations that can be adopted by the linked tetrahedra. As a result, the repeat distance along the *c*-axis can be 2, 3, ..., 7, 9, or 12 tetrahedra. We have considered the pyroxene minerals enstatite ($Mg_2Si_2O_6$), jadeite ($NaAlSi_2O_6$), and spodumene ($LiAlSi_2O_6$), the synthetic metasilicates $Li_2SiO_3$ and $Na_2SiO_3$, and wollastonite ($Ca_2Si_3O_9$). Typical errors are within 2% for cell parameters and average distances, while calculated mechanical properties have higher errors with respect to the experimental ones.

*3.2.5. Phyllosilicates.* We have considered silicates with a layer structure of the formula $M_2Si_2O_5$ (M = Li, Na). Typical errors within 1.5% have been found in the structure. No experimental data are available for mechanical properties. It is worth noting that in these structures the ratio between the bridging oxygen and the nonbridging oxygen is 3:1 and the average Si—O distance is better reproduced, with an error within 1%. Despite the fact that $K_2Si_2O_5$ is not a phyllosilicate, we have added it in Table 10 because, as previously mentioned, the Li—O, Na—O, and K—O interactions have been parametrized using the structures of the alkali disilicate reported in Table 10.

*3.2.6 Tectosilicates.* We have considered two minerals, namely, $KAlSi_3O_8$ (microcline) and $NaAlSi_3O_8$ (albite), which are constructed from $SiO_4$ units with O atoms shared by two tetrahedra (as in the various forms of $SiO_2$ itself) and up to one-half of the Si atoms replaced by Al, thus requiring the addition of further cations to guarantee the electro-neutrality. In this case, the average Si—O distances are predicted with an error about 0.5%. The average Al—O distances are also reproduced with an error about 0.5%, while the errors in cell parameters are below 1.5%.

**3.3. Glass Structure.** Table 12 shows the comparison of bond length values obtained in this work with those obtained in previous simulations. Moreover, a comparison with the experimental results provided by neutron diffraction and EXAFS studies is also reported. The bond lengths have been calculated according to the method reported by Yuan and Cormack.[31] For the Si—O, O—O, and Si—Si pairs, the peak positions have been calculated by analyzing the full width at half-maximum (fwhm) of the calculated pair correlation functions broadened with $Q_{max}$ = 45.2 Å$^{-1}$. The most probable distance of the Na—O pair distribution function has been taken as the bond length.

*3.3.1. Local Structures in Sodium Silicate Glasses.* Table 12 lists the results obtained by using the potentials derived in this

**TABLE 8: Structural and Mechanical Properties for Selected Crystal Silicates (Cyclosilicates)**

| | | lattice parameters | | | | | | | | elastic constants ($10^{10}$ Pa) | | | | | | | | | | |
|---|---|---|---|---|---|---|---|---|---|---|---|---|---|---|---|---|---|---|---|---|
| | | $a$ (Å) | $b$ (Å) | $c$ (Å) | $\gamma$ (deg) | $V_{cell}$ (Å$^3$) | <Si−O> | <M−O> | <MI−O> | $C_{11}$ | $C_{22}$ | $C_{33}$ | $C_{44}$ | $C_{55}$ | $C_{66}$ | $C_{12}$ | $C_{13}$ | $C_{14}$ | $C_{23}$ | $B$ |
| Be$_3$Al$_2$(SiO$_3$)$_6$ | expt | 9.2090 | 9.2090 | 9.1970 | 120 | 675.463 | 1.5974 | 1.6555 | 1.9163 | 30.85 | | 28.34 | 6.61 | | | 12.89 | 11.85 | | | 18.10 |
| beryl | calcd | 9.2018 | 9.2018 | 9.2778 | 120 | 680.337 | 1.5922 | 1.6694 | 1.9459 | 30.28 | | 28.12 | 4.69 | | | 13.01 | 11.06 | | | 17.59 |
| | % error | −0.08 | −0.08 | 0.88 | 0 | 0.7 | −0.3 | 0.8 | 1.5 | −1.8 | | −0.8 | −29 | | | 0.9 | −6.7 | | | −2.8 |
| BaTi(SiO$_3$)$_3$ | expt | 6.6410 | 6.6410 | 9.7600 | 120 | 372.776 | 1.6242 | 2.7668 | 1.9427 | | | | | | | | | | | |
| benitoite | calcd | 6.7157 | 6.7157 | 9.8804 | 120 | 385.913 | 1.6088 | 2.8857 | 1.9532 | | | | | | | | | | | |
| | % error | 1.1 | 1.1 | 1.2 | 0 | 3.5 | −0.9 | 4.3 | 0.5 | | | | | | | | | | | |
| Na$_2$Be$_2$(SiO$_3$)$_3$ | expt | 11.7480 | 9.4150 | 6.8180 | 90 | 754.121 | 1.6224 | 2.6314 | 1.6291 | | | | | | | | | | | |
| | calcd | 11.7355 | 9.4594 | 6.7974 | 90 | 754.583 | 1.6068 | 2.6649 | 1.6340 | | | | | | | | | | | |
| | % error | −0.1 | 0.5 | −0.3 | 0 | 0.06 | −0.96 | 1.3 | 0.3 | | | | | | | | | | | |

**TABLE 9: Structural and Mechanical Properties for Selected Crystal Silicates (Inosilicates)**

| | | lattice parameters | | | | | | | | | | elastic constants ($10^{10}$ Pa) | | | | | | | | | | |
|---|---|---|---|---|---|---|---|---|---|---|---|---|---|---|---|---|---|---|---|---|---|---|
| | | $a$ (Å) | $b$ (Å) | $c$ (Å) | $\alpha$ (deg) | $\beta$ (deg) | $\gamma$ (deg) | $V_{cell}$ (Å$^3$) | <Si−O> | <Al−O> | <M−O> | $C_{11}$ | $C_{22}$ | $C_{33}$ | $C_{44}$ | $C_{55}$ | $C_{66}$ | $C_{12}$ | $C_{13}$ | $C_{14}$ | $C_{23}$ | $B$ |
| NaAlSi$_2$O$_6$ | expt | 9.4180 | 8.5620 | 5.2190 | 90 | 107.97 | 90 | 400.315 | 1.6213 | 1.9273 | 2.4665 | 27.4 | 25.3 | 28.2 | 8.8 | 6.5 | 9.4 | 9.4 | 7.1 | | 8.2 | 14.3 |
| jadeite | calcd | 9.4274 | 8.5110 | 5.2963 | 90 | 107.94 | 90 | 404.297 | 1.6016 | 1.9594 | 2.5034 | 25.59 | 25.86 | 28.18 | 9.43 | 7.27 | 5.99 | 8.17 | 8.16 | | 11.3 | 14.84 |
| | % error | 0.1 | −0.6 | 1.5 | 0 | 0.03 | 0 | 1.0 | −1.2 | 1.67 | 1.5 | −6.6 | 2.2 | −0.07 | 7.2 | 11.8 | −36 | −13 | 15 | | 38 | 3.8 |
| LiAlSi$_2$O$_6$ | expt | 9.4630 | 8.3920 | 5.2180 | 90 | 110.15 | 90 | 389.017 | 1.6191 | 1.9208 | 2.2128 | 24.5 | 19.9 | 28.7 | 7.01 | 6.28 | 7.07 | 8.8 | 6.4 | | 6.9 | 12.35 |
| spodumene | calcd | 9.4912 | 8.2439 | 5.3055 | 90 | 110.00 | 90 | 390.170 | 1.5992 | 1.9475 | 2.2293 | 24.83 | 20.57 | 26.66 | 9.63 | 10.28 | 4.87 | 9.82 | 11.78 | | 10.96 | 14.95 |
| | % error | 0.3 | −1.8 | 1.7 | 0 | −0.16 | 0 | 0.3 | −1.2 | 1.4 | 0.7 | 1.3 | 3.4 | −7.1 | 37 | 64 | −31 | 11.6 | 84 | | 59 | 21.1 |
| Mg$_2$Si$_2$O$_6$ | expt | 18.2350 | 8.8180 | 5.1790 | 90 | 90 | 90 | 832.764 | 1.6340 | | 2.1149 | 22.47 | 17.79 | 21.36 | 7.76 | 7.59 | 8.16 | 7.24 | 5.41 | | 5.27 | 10.78 |
| estatite | calcd | 18.5219 | 8.8489 | 5.2582 | 90 | 90 | 90 | 861.805 | 1.6054 | | 2.0727 | 20.29 | 11.52 | 15.57 | 6.83 | 6.16 | 5.35 | 5.01 | 3.28 | | 1.46 | 6.84 |
| | % error | 1.57 | 0.35 | 1.5 | 0 | 0 | 0 | 3.5 | −1.75 | | −2.0 | −9.7 | −35 | −27 | −12 | −19 | −34 | −31 | −39 | | −72 | −37 |
| Ca$_3$Si$_3$O$_9$ | expt | 7.9400 | 7.3200 | 7.07 | 90.3 | 95.37 | 103.43 | 397.769 | 1.6227 | | 2.4003 | | | | | | | | | | | |
| wollastonite | calcd | 7.8177 | 7.3330 | 7.126 | 90.1 | 92.82 | 103.54 | 396.641 | 1.6020 | | 2.4454 | | | | | | | | | | | |
| | % error | −1.5 | 0.18 | 0.8 | −0.2 | −2.7 | 0.1 | −0.3 | −1.3 | | 1.9 | | | | | | | | | | | |
| Na$_2$SiO$_3$ | expt | 10.4800 | 6.0700 | 4.8200 | 90 | 90 | 90 | 306.618 | 1.6381 | | 2.3813 | | | | | | | | | | | |
| | calcd | 10.5754 | 5.9556 | 4.8264 | 90 | 90 | 90 | 304.039 | 1.6096 | | 2.4039 | | | | | | | | | | | |
| | % error | 0.9 | −1.9 | 0.1 | 0 | 0 | 0 | −0.8 | −1.7 | | 0.9 | | | | | | | | | | | |
| Li$_2$SiO$_3$ | expt | 9.3960 | 5.3960 | 4.6610 | 90 | 90 | 90 | 236.317 | 1.6408 | | 2.0016 | | | | | | | | | | | |
| | calcd | 9.4656 | 5.3726 | 4.7286 | 90 | 90 | 90 | 240.470 | 1.6140 | | 2.0406 | | | | | | | | | | | |
| | % error | 0.7 | −0.4 | 1.45 | 0 | 0 | 0 | 1.8 | −1.6 | | 1.9 | | | | | | | | | | | |

**TABLE 10: Structural and Mechanical Properties for Selected Crystal Silicates (Phyllosilicates)**

| | | lattice parameters | | | | | | | | elastic constants ($10^{10}$ Pa) | | | | | | | | | | |
|---|---|---|---|---|---|---|---|---|---|---|---|---|---|---|---|---|---|---|---|---|
| | | $a$ (Å) | $b$ (Å) | $c$ (Å) | $\alpha$ (deg) | $\beta$ (deg) | $\gamma$ (deg) | $V_{cell}$ (Å³) | <Si−O> | <M−O> | $C_{11}$ | $C_{22}$ | $C_{33}$ | $C_{44}$ | $C_{55}$ | $C_{66}$ | $C_{12}$ | $C_{13}$ | $C_{14}$ | $C_{23}$ | $B$ |
| Na₂Si₂O₅ | expt | 6.4090 | 15.4220 | 4.8960 | 90 | 90 | 90 | 483.919 | 1.6160 | 2.3974 | | | | | | | | | | | |
| | calcd | 6.3042 | 15.4289 | 4.9626 | 90 | 90 | 90 | 482.698 | 1.6036 | 2.4116 | | | | | | | | | | | |
| | % error | −1.6 | 0.04 | 1.36 | 0 | 0 | 0 | −0.25 | −0.76 | 0.6 | | | | | | | | | | | |
| Li₂Si₂O₅ | expt | 5.6830 | 4.7840 | 14.6480 | 90 | 90 | 90 | 398.242 | 1.6182 | 1.9987 | | | | | | | | | | | |
| | calcd | 5.6244 | 4.8754 | 14.6526 | 90 | 90 | 90 | 401.793 | 1.6054 | 2.0181 | | | | | | | | | | | |
| | % error | −1.0 | 1.9 | 0.03 | 0 | 0 | 0 | 0.9 | −0.8 | 0.97 | | | | | | | | | | | |
| K₂Si₂O₅[a] | expt | 16.3224 | 11.2430 | 9.9190 | 90 | 115.97 | 90 | 1636.459 | 1.6235 | 2.8500 | | | | | | | | | | | |
| | calcd | 16.4127 | 11.2904 | 9.8247 | 90 | 114.16 | 90 | 1661.119 | 1.6061 | 2.8952 | | | | | | | | | | | |
| | % error | 0.6 | 0.4 | −0.95 | 0 | −1.6 | 0 | 1.5 | −1.07 | 1.6 | | | | | | | | | | | |

[a] K₂Si₂O₅ is not a phyllosilicate, we have included it here because, as previously mentioned, the Li−O, Na−O, and K−O interactions were parametrized using the structures of the alkali disilicate.

**TABLE 11: Structural and Mechanical Properties for Selected Crystal Silicates (Tectosilicates)**

| | | lattice parameters | | | | | | | | | | elastic constants ($10^{10}$ Pa) | | | | | | | | | | |
|---|---|---|---|---|---|---|---|---|---|---|---|---|---|---|---|---|---|---|---|---|---|---|
| | | $a$ (Å) | $b$ (Å) | $c$ (Å) | $\alpha$ (deg) | $\beta$ (deg) | $\gamma$ (deg) | $V_{cell}$ (Å³) | <Si−O> | <Al−O> | <M−O> | $C_{11}$ | $C_{22}$ | $C_{33}$ | $C_{44}$ | $C_{55}$ | $C_{66}$ | $C_{12}$ | $C_{13}$ | $C_{14}$ | $C_{23}$ | $B$ |
| KAlSi₃O₈ | expt | 7.9205 | 7.6219 | 7.2188 | 76.55 | 104.38 | 66.87 | 360.56 | 1.6446 | 1.6557 | 2.9262 | 6.7 | 16.9 | 11.8 | 1.43 | 2.38 | 3.64 | 4.53 | 2.65 | | 2.04 | 5.54 |
| microcline | calcd | 7.7892 | 7.5786 | 7.2248 | 78.95 | 105.56 | 61.6 | 334.79 | 1.6360 | 1.6468 | 2.9378 | 13.96 | 7.72 | 13.13 | 3.47 | 2.79 | 3.31 | 4.12 | 2.87 | | 3.07 | 4.41 |
| | % error | −1.66 | −0.57 | 0.08 | 3.1 | 1.1 | −7.9 | −7.1 | −0.5 | −0.5 | 0.4 | 108 | −54 | 11.3 | 142 | 17.2 | −9.1 | −9.1 | 8.3 | | 50.5 | −20 |
| CaAl₂Si₂O₈ | expt | 8.1750 | 12.8730 | 14.1700 | 93.11 | 115.89 | 91.28 | 1337.804 | 1.6209 | 1.7412 | 2.4982 | 12.4 | 20.5 | 15.6 | 2.35 | 4.04 | 4.15 | 6.6 | 5.0 | | 4.2 | 8.42 |
| anorthite | calcd | 7.9151 | 12.9053 | 14.0846 | 93.49 | 115.68 | 91.67 | 1291.74 | 1.5989 | 1.7302 | 2.4837 | 10.0 | 18.0 | 17.17 | 3.61 | 3.75 | 3.12 | 4.94 | 6.33 | | 4.32 | 7.73 |
| | % error | −3.1 | 0.25 | −0.6 | 0.4 | −0.2 | 0.4 | −3.4 | −1.35 | −0.6 | −0.6 | −19.3 | −12. | 10.0 | 53.6 | −7.2 | −25 | −25 | 26.6 | | 2.9 | −8.2 |
| NaAlSi₃O₈ | expt | 8.1520 | 12.8310 | 7.1100 | 93.46 | 116.52 | 89.72 | 664.026 | 1.6391 | 1.6391 | 2.5290 | 7.40 | 13.1 | 12.8 | 1.73 | 2.96 | 3.20 | 3.64 | 3.94 | | 3.1 | 5.69 |
| albite | calcd | 8.0500 | 12.6704 | 7.0210 | 93.46 | 116.52 | 89.72 | 639.404 | 1.6312 | 1.6312 | 2.5298 | 6.67 | 16.1 | 15.36 | 1.66 | 3.49 | 2.94 | 3.46 | 4.70 | | 1.1 | 5.46 |
| | % error | −1.25 | −1.25 | −1.25 | 0 | 0 | 0 | −3.7 | −0.5 | −0.5 | 0.03 | −9.9 | 22.9 | 20 | −4.0 | 17.9 | −8.1 | −4.9 | 19 | | −63 | −4.0 |

**TABLE 12: Comparison of Bond Lengths of the Simulated Glasses with Different Interatomic Potentials and Experimental Studies**

| | Na$_2$O % | MD this work[a] | MD Du[b] | MD Yuan[c] | neutron[d] | EXAFS[e] |
|---|---|---|---|---|---|---|
| Si$-$O | $x = 0$ | 1.616 | 1.620/1.619 | 1.616/1.615 | 1.610/1.608 | 1.608 |
| | $x = 10$ | 1.618 | 1.615 | 1.615 | | |
| | $x = 15$ | 1.617 | | | | |
| | $x = 20$ | 1.616 | 1.615 | 1.614 | 1.617 | 1.617 |
| | $x = 25$ | 1.615 | | | | |
| | $x = 30$ | 1.614 | 1.611 | 1.613 | 1.622 | 1.668 |
| Si$-$BO/Si$-$NBO | $x = 0$ | 1.616 | | | | |
| | $x = 10$ | 1.621/1.550 | | | | |
| | $x = 15$ | 1.622/1.553 | | | | |
| | $x = 20$ | 1.624/1.554 | | | | |
| | $x = 25$ | 1.626/1.556 | | | | |
| | $x = 30$ | 1.628/1.559 | | | | |
| O$-$O | $x = 0$ | 2.624 | 2.624/2.617 | 2.626/2.621 | 2.629/2.626 | |
| | $x = 10$ | 2.626 | 2.628 | 2.622 | | |
| | $x = 15$ | 2.624 | | | | |
| | $x = 20$ | 2.624 | 2.624 | 2.622 | | |
| | $x = 25$ | 2.624 | | | | |
| | $x = 30$ | 2.623 | 2.624 | 2.608 | | |
| Si$-$Si | $x = 0$ | 3.140 | 3.146/3.159 | 3.129 | 3.077/3.077 | |
| | $x = 10$ | 3.149 | 3.146 | 3.140 | | |
| | $x = 15$ | 3.146 | | | | |
| | $x = 20$ | 3.150 | 3.142 | 3.142 | | |
| | $x = 25$ | 3.148 | | | | |
| | $x = 30$ | 3.149 | 3.146 | 3.139 | | |
| Na$-$O | $x = 10$ | 2.307 | 2.362 | 2.31 | | 2.32 |
| | $x = 15$ | 2.288 | | | | |
| | $x = 20$ | 2.312 | 2.382 | 2.32 | 2.36 | 2.30 |
| | $x = 25$ | 2.332 | | | | |
| | $x = 30$ | 2.323 | 2.388 | 2.33 | 2.36 | |

[a] Results obtained using the interatomic potential developed in this work. The values listed are an average upon three simulations starting from different initial configurations. [b] Data from Du and Cormack.[43] [c] Data from Yuan and Cormack.[31] [d] Neutron diffractions are from Wright et al.[52] and Clare et al.[55] with $Q_{max}$ of 22.88 Å$^{-1}$, and that of silica is from Grimley et al.[54] with $Q_{max}$ of 45.2 Å$^{-1}$ and where indicated after the slash.[e] Si$-$O bond lengths are from Henderson;[56] Na$-$O data are from Greaves et al.[57] and Mazzara et al.[58]

work and those obtained by Cormack et al.[31,43] by making use of the Buckingham function and the same ionic charge scheme adopted in this work. Our results agree with those obtained by Cormack et al.,[31,43] for both the short-range and the medium-range orders with respect to the Si$-$O backbone network structure. All the simulations reported in Table 12 predict that the average Si$-$O bond length become shorter by increasing the sodium content in the glass. The Si$-$O bond length decreases slightly from 1.618 to 1.614 Å passing from NS10 to NS30. This result apparently contradicts the experimental data obtained from neutron diffraction experiments by Wright et al.[53] They found that the Si$-$O bond length increases from 1.617 to 1.622 Å for glasses with 22 and 31 mol % Na$_2$O concentrations, respectively. We note, however, that although the average Si$-$O bond length decreases, both Si$-$NBO and Si$-$BO bond lengths increase with sodium concentration: The Si$-$BO bond length increases from 1.621 to 1.628 Å, while the Si$-$NBO bond length increases from 1.550 to 1.559 Å. The Si$-$NBO distance is nearly 0.069 Å shorter than the Si$-$BO bond lengths. These findings are in agreement with the differences of Si$-$BO and Si$-$NBO bond lengths in the $\alpha$-Na$_2$Si$_2$O$_5$ and Na$_2$SiO$_3$ crystal phases, which are 0.06 and 0.08 Å, respectively.[59] The average Si$-$O bond length decreases because the NBO content increases with Na concentration and the increase of the bond length values of both components is not sufficient to invert the trend. In fact, the intensity of the BO peaks decreases while, at the same time, the NBO peak increases. These observations were attributed by Yuan and Cormack to the lack of distinct charge assignments for BO and NBO in the potential model.[31] This trend is found also in modeling silicate crystals, as discussed previously in section 3.2.1.1. In fact, the negative errors associated with the Si$-$O bond lengths decrease from 2% in nesosilicates to 0.5%

in tectosilicates. The error increase depends on the increase of the NBO/BO ratio in the system. The addition of sodium oxide produces an increase of the ionic character of the Si$-$O bond, and it could be more appropriate to use a variable charge potential model[15] to reproduce the experimental data.

The O$-$O bond length is 2.624 Å and does not seem to change with the addition of sodium oxide. This value is in agreement with the neutron diffraction data of 2.629 Å.[53]

The Na$-$O bond lengths range from 2.300 to 2.332 Å, and the pair distribution function shows that the Na$-$O peak increases and becomes sharper with the addition of Na$_2$O (Figure 1a). These results agree well with EXAFS and neutron diffraction data for which the Na$-$O bond lengths range from 2.30 to 2.36 Å.[55,57,58]

The coordination number of the sodium ions increases from 4.32 to 4.78 for NS10 and NS30 glasses, and it tends to 5 for the Na$_2$Si$_2$O$_5$ glass (Table 13). Accordingly, Greaves et al.[56] also found that 5 ± 0.5 O ions are around Na for sodium disilicate glasses.

The NBO/BO ratio around Na increases with the sodium oxide content, it ranges from 0.82 to 2.14, and the BO/NBO ratio around Si is 3.65 for NS30 glass, while both the ratio values are 4 in the crystalline Na$_2$Si$_2$O$_5$.[59]

All these observations show that the average local environment around the Na ions becomes more ordered with the addition of Na$_2$O. This is demonstrated also by analyzing the O$-$Na$-$O bond angle distribution, Figure 1b. As already discussed by Cormack et al.,[31,43] this distribution features a distinct peak at 60°, a broad peak at around 90°, and a shoulder at 150°.

Table 14 reports peak positions and fwhm's of O$-$Si$-$O and Si$-$O$-$Si bond angle distributions. The O$-$Si$-$O angle in-
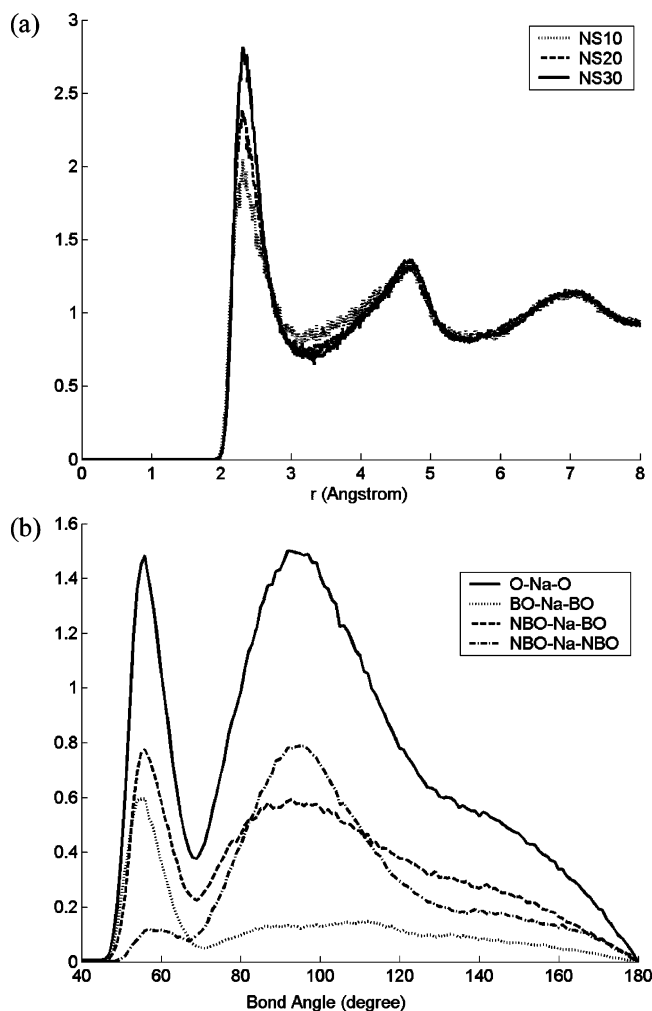
(a)



(b)



**Figure 1.** (a) Na−O pair distribution functions for the sodium silicate glasses simulated. We have reported only the NS10, NS20, and NS30 glasses for clarity (b) Bond angle distribution function O−Na−O for NS30 glass and BO and NBO contributions.

**TABLE 13: Coordination Numbers and Their BO and NBO Contributions**[a]

|        | NS10 | NS15 | NS20 | NS25 | NS30 |
|--------|------|------|------|------|------|
| Si−O   | 4.00 | 4.00 | 4.00 | 4.00 | 4.00 |
| Si−BO  | 3.78 | 3.65 | 3.50 | 3.33 | 3.14 |
| Si−NBO | 0.22 | 0.35 | 0.50 | 0.67 | 0.86 |
| Na−O   | 4.32 | 4.46 | 4.60 | 4.71 | 4.78 |
| Na−BO  | 2.37 | 2.02 | 1.88 | 1.68 | 1.52 |
| Na−NBO | 1.95 | 2.44 | 2.72 | 3.03 | 3.26 |

[a] The cutoffs were set to 1.8 and 3.0 Å for the Si−O and Na−O pairs, respectively.

**TABLE 14: Bond Angle Distributions of Silica and Sodium Silicate Glasses**

|         | O−Si−O (deg) | | Si−O−Si (deg) | |
|---------|------|------|------|------|
|         | peak | fwhm | peak | fwhm |
| SiO₂    | 108.6 | 13.5 | 153.5 | 34 |
| NS10    | 108.7 | 13.0 | 153.6 | 34.5 |
| NS15    | 108.8 | 12.7 | 152.7 | 33.5 |
| NS20    | 108.9 | 12.2 | 152.8 | 32.5 |
| NS25    | 109.0 | 12.0 | 151.0 | 33.8 |
| NS30    | 109.0 | 11.3 | 150.6 | 33.7 |

creases from 108.6° for silica to 109.0° for NS30 glass, while the fwhm decreases from 13.5° to 11.2°. These results agree well with those obtained by means of neutron diffraction studies by Mitsawa et al.[64] They reported a slight increase of the

O−Si−O angle from 109.1° for silica to 109.3° for sodium disilicate glass. The SiO₄ tetrahedra reach a more regular geometry when the network is depolymerized.

To our knowledge no experimental data are available for the Si−O−Si angle distribution in sodium silicate glasses. High-energy X-ray studies of silica[65] show the Si−O−Si peak position and fwhm to be 147° and 35°, respectively, in agreement with the results of two-dimensional ¹⁷O dynamic-angle spinning NMR[66] spectroscopy, which estimated the peak position of the Si−O−Si angle to be 146.7° ± 3.8°. The results obtained in this study show that the peak positions of the Si−O−Si bond angle distribution decreases from 153.5° for silica to 150.6° for NS30 glass. As previously suggested, the overestimation of this angle might be due to the limited size of the simulation box utilized and lack of polarizability effects in the calculations.[18]

*3.3.2. Mechanical Properties..* Table 15 lists the $E$, $G$, $B$, and $\nu$ values obtained in this work by averaging upon three simulation runs, together with those predicted using the different empirical methods included into the SciGlass package[49] and together with experimental data.[47] The percent errors are reported in brackets. We have chosen the empirical models that provide the best agreement with the experimental data. These are incremental models, valid within limited concentration ranges, namely, Appen's method,[67] Gan Fuxi's method,[68] Demkina's method,[69] and Priven's method.[70]

The agreement of the results obtained from the simulations with the experimental data is good. The Young's modulus decreases upon the addition of sodium oxide because of the decrease in the polymerization of the silica network. In fact, the elastic modulus $E$ is determined by the individual bonds in the material and by the structure of the network (intermediate range order). The shear modulus $G$ decreases with Na₂O concentration, and it is slightly underestimated, as is the Young modulus $E$. However, in both cases the errors are within 6%. However, both the bulk modulus and the Poisson's ratio increase with Na₂O concentration. This might be due to the fact that upon the addition of Na₂O the total free volume decreases, while the density of packing of the atoms in the structure increases leading to a lower compressibility of the material and to a higher bulk modulus. The relative errors of both $B$ and $\nu$ are overestimated by 7% and 15%, respectively.

**3.4. Alumino-Phosphate.** A good test for the transferability of a new interatomic potential is to compare the computed structural and mechanical properties of a compound that has not been explicitly considered during the parametrization procedure. We have chosen the alumino-phosphate AlPO₄ berlinite because of its interest and of the presence of previous calculations with different potential models.[38,39,71] In fact, in the past few decades, many researchers focused their attention on the wide class of zeolite minerals. Their rich polymorphism, combined with their technological importance as selective catalysts and adsorbents, has induced a widespread interest in the physical and chemical properties of these systems. Therefore, nowadays many force fields are available in the literature.[38,39,71]

Table 16 reports the structural and mechanical properties and static dielectric constants calculated using the force field derived in this study. They are compared with experimental data[72−74] and with the results calculated by means of two of the force fields more widely used. Gale and Henson[39] used Buckingham functions and treated the polarizability of the oxygen atoms using the shell model developed by Dick and Overhauser.[75] They used Catlow's parameters[76] for the O−O interaction and derived the P−O parameters by empirical fitting of the crystal structure and the elastic and dielectric properties of berlinite. Kramer et

Empirical Interatomic Potential Model for Glasses

*J. Phys. Chem. B, Vol. 110, No. 24, 2006* **11793**

**TABLE 15: Comparison of Mechanical Properties ($E$ = Young's Modulus, $G$ = Shear Modulus, $B$ = Bulk Modulus and $\nu$ = Poisson's Ratio) Calculated by Means of Free Energy Minimizations ($T$ = 300 K and $P$ = 1 atm) with Experimental Data from Ref 47 and Those Predicted by Means of Different Empirical Methods Available in the SciGlass Package[49]**

|  | Na$_2$O % | experimental | this work | Appen | Demkina 76 | Gan Fuxi | Priven 2000 |
|---|---|---|---|---|---|---|---|
| $E$ (GPa) | $x = 0$ | 72.50[a] | 72.05 (−0.6) | 70.24 (−3.1) | 66.42 (−8.4) | 71.83 (−0.9) | 68.00 (−6.2) |
|  | $x = 10$ | 65.29 | 64.20 (−1.7) | 66.06 (1.2) | 66.27 (1.5) | 67.05 (2.7) | 59.30 (−9.2) |
|  | $x = 15$ | 62.90 | 61.07 (−2.9) | 64.12 (1.9) | 66.19 (5.2) | 64.85 (3.1) | 62.45 (−0.7) |
|  | $x = 20$ | 61.08 | 58.53 (−4.2) | 62.27 (1.9) | 66.09 (8.2) | 62.76 (2.8) | 60.60 (−0.8) |
|  | $x = 25$ | 59.77 | 58.13 (−2.7) | 60.53 (1.3) | 65.99 (10.4) | 60.80 (1.7) | 58.75 (−1.7) |
|  | $x = 30$ | 59.33 | 56.64 (−4.5) | 58.58 (−1.3) | 65.88 (11.0) | 58.96 (−0.6) | 56.90 (−4.1) |
| $G$ (GPa) | $x = 0$ | 31.25[a] | 30.43 (−2.6) | 29.72 (−4.9) | 28.49 (−8.8) | 31.18 (−0.2) | 29.06 (−7.0) |
|  | $x = 10$ | 27.68 | 26.99 (−2.5) | 27.34 (−1.2) | 28.15 (1.7) | 28.48 (2.9) | 24.87 (−10.2) |
|  | $x = 15$ | 26.29 | 25.11 (−4.5) | 26.22 (−0.3) | 27.98 (6.4) | 27.23 (3.6) | 26.19 (−0.4) |
|  | $x = 20$ | 25.18 | 23.60 (−6.3) | 25.15 (−0.1) | 27.81 (10.4) | 26.04 (3.4) | 25.27 (−0.4) |
|  | $x = 25$ | 24.26 | 23.26 (−4.1) | 24.13 (−0.5) | 27.65 (14.0) | 24.91 (2.7) | 24.36 (−0.4) |
|  | $x = 30$ | 23.80 | 22.38 (−6.0) | 23.16 (−2.7) | 27.48 (15.5) | 23.85 (0.2) | 23.46 (−1.4) |
| $B$ (GPa) | $x = 0$ | 36.10[a] | 37.94 (5.1) | 36.76 (1.8) | 33.11 (−8.3) | 34.41 (−4.7) | 34.34 (−4.9) |
|  | $x = 10$ | 33.95 | 34.67 (2.1) | 37.72 (11.1) | 34.20 (0.7) | 34.62 (2.0) | 34.08 (0.4) |
|  | $x = 15$ | 34.51 | 35.57 (3.1) | 38.52 (11.6) | 34.76 (0.7) | 34.96 (1.3) | 33.84 (−1.9) |
|  | $x = 20$ | 35.46 | 37.18 (4.9) | 39.60 (11.7) | 35.32 (−0.4) | 35.48 (0.0) | 33.58 (−5.0) |
|  | $x = 25$ | 37.16 | 38.52 (3.7) | 41.02 (10.4) | 35.88 (−3.4) | 36.22 (−2.5) | 33.30 (10.4) |
|  | $x = 30$ | 39.03 | 40.13 (2.8) | 42.87 (9.8) | 36.46 (−6.6) | 37.22 (−4.6) | 33.02 (−15.4) |
| $\nu$ | $x = 0$ | 0.160[a] | 0.184 (15.0) |  | 0.166 (3.8) |  | 0.170 (6.3) |
|  | $x = 10$ | 0.180 | 0.191 (6.1) |  | 0.177 (−0.3) |  | 0.186 (3.3) |
|  | $x = 15$ | 0.196 | 0.216 (10.2) |  | 0.183 (−6.6) |  | 0.192 (−2.0) |
|  | $x = 20$ | 0.213 | 0.240 (12.7) |  | 0.188 (−11.7) |  | 0.199 (−6.6) |
|  | $x = 25$ | 0.232 | 0.250 (7.8) |  | 0.194 (−16.4) |  | 0.206 (−11.2) |
|  | $x = 30$ | 0.247 | 0.265 (7.3) |  | 0.199 (−19.4) |  | 0.213 (−13.8) |

[a] Elastic constants for SiO$_2$ glass have been taken from ref 48, and $G$ was calculated by means of eq 9.

**TABLE 16: Comparison of Experimental and Calculated Structures and Properties for AlPO$_4$ Berlinite with Different Potential Models ($T$ = 300K and $P$ = 1 atm)**

|  | exptl[a] | Gale and Henson[39] | Kramer et al.[38] | this work |
|---|---|---|---|---|
| $a$ (Å) | 4.9423 | 4.9117 | 5.0111 | 4.9448 |
| $c$ (Å) | 10.9446 | 10.9576 | 11.1424 | 10.9833 |
| Al, $x$ | 0.4664 | 0.4671 | 0.4672 | 0.4547 |
| P, $x$ | 0.4669 | 0.4699 | 0.4656 | 0.4541 |
| O(1), $x$ | 0.4163 | 0.4083 | 0.4331 | 0.4308 |
| O(1), $y$ | 0.2922 | 0.2890 | 0.2907 | 0.3043 |
| O(1), $z$ | 0.3977 | 0.4973 | 0.4035 | 0.3983 |
| O(2), $x$ | 0.4156 | 0.4179 | 0.4232 | 0.4172 |
| O(2), $y$ | 0.2576 | 0.2599 | 0.2486 | 0.2639 |
| O(2), $z$ | 0.8837 | 0.8823 | 0.8903 | 0.8851 |
| <Al−O> | 1.7358 | 1.7351 | 1.7398 | 1.7339 |
| <P−O> | 1.5213 | 1.5212 | 1.5081 | 1.5194 |
| $V_{cell}$ (Å$^3$) | 231.5201 | 228.9378 | 242.3105 | 232.5725 |
| $C_{11}$ (10$^{10}$ Pa) | 6.98 | 8.19 | 8.40 | 6.92 |
| $C_{33}$ (10$^{10}$ Pa) | 8.71 | 10.69 | 9.69 | 10.18 |
| $C_{44}$ (10$^{10}$ Pa) | 4.22 | 4.41 | 4.68 | 3.98 |
| $C_{12}$ (10$^{10}$ Pa) | 1.06 | 1.59 | 0.93 | 1.24 |
| $C_{13}$ (10$^{10}$ Pa) | 1.49 | 2.22 | 1.57 | 1.41 |
| $C_{14}$ (10$^{10}$ Pa) | 1.34 | 1.09 | 1.35 | 1.28 |
| $B$ (10$^{10}$ Pa) | 3.39 | 4.25 | 3.81 | 3.46 |
| $\epsilon^0_{11}$ | 5.47 | 5.25 | 1.92 | 2.08 |
| $\epsilon^0_{33}$ | 5.37 | 5.42 | 1.94 | 2.11 |

[a] The trigonal symmetry class with space group $P3_121$ has been taken from Thong and Schwarzenbach;[72] mechanical properties based on Brillouin scattering are from ref 73, and static dielectric constants are from ref 74.

al.[38] used a rigid ionic model with partial charges, and the parameters of the Buckingham functional form for the short-range interactions were derived by fitting to the potential energy surface of small clusters of H$_4$TO$_4$ (T = Si, Al, P) to represent the building blocks of zeolites.

Despite the fact that our potentials were derived by empirical fitting of crystal structures and elastic properties of binary oxides (α-Al$_2$O$_3$ and P$_4$O$_{10}$ for Al−O and P−O interactions, respectively), our results on berlinite structural and mechanical properties are similar to those calculated with Kramer's potentials. Both Kramer's potentials and our force field fail in simulating dielectric properties because they adopt the rigid ionic model. However, even within this approximation, structural and mechanical properties are in good agreement with experimental data and with those calculated with the potential developed by Gale and Henson.

## 4. Conclusions

A self-consistent pairwise interatomic potential has been developed by means of empirical fitting on structural parameters and elastic constants of binary oxides using free energy minimization at $T$ = 300 K and $P$ = 1 atm.

A rigid ionic potential model has been used, and a partial charge $q_O = -1.2e$ has been assigned to the oxygen atom. Despite the fact that the O−O interaction has been fitted on α-quartz, this provides good results also for other oxides in which different covalency is present. These differences are subsumed in the M−O parameters that were subsequently fitted on binary oxides.

The potential derived in this work has been shown to be able to reproduce structural parameters and mechanical properties of a wide range of crystal silicates and glasses.

The Si−O average distances have been found to be shorter than the experimental ones in all the cases that we have studied, and the errors increase with the NBO/BO ratio in the glasses. This result is expected, since the Si−O interaction has been derived from α-quartz that is a tectosilicate with no NBO oxygens. The potential model could be improved by taking into account different charges for bridging and nonbridging oxygens in a variable charge potential model.

Thanks to the choice of a pairwise partial charge model, the computational effort required in the evaluation of forces is reduced with respect to a three-body term potential, a variable charge model,[14,15] or a core−shell model.[71] In addition, no assumptions are made about the coordination number of the

cations. In fact, since a two-body potential is employed, the cations are allowed to change their coordination depending on the environment in which they are placed. For instance, the Al−O interaction has been parametrized on corundum in which Al is 6-fold coordinated with average bond length distances of 1.913 Å. However, the environment around Al is well reproduced both in AlPO$_4$ berlinite in which Al is 4-fold coordinated and other alumino-silicates in which Al can occupy 4-, 5-, and 6-fold sites.

The force field that we have obtained in this work could be further refined by considering additional properties besides structural end elastic parameters, but the choice can be hindered by the availability of experimental data. However, ab initio simulation of complex materials has now reached a level of excellent accuracy not only with respect to structures but also as far as dynamical features are concerned, such as vibrational frequencies.[77,78] Therefore, it could be possible, in the future, to consider also this a source of accurate data to refine classical force fields.

Finally, the calculations performed on the sodium silicate glass are very promising; further work has been devoted to similar alkaline silicate glasses, and it will be reported in near future. Moreover, it is worth noting that the potential derived in this study is able to reproduce structural and mechanical properties of alumino-phosphates, although they have not explicitly considered during the parametrization procedure.

## References and Notes

(1) Shelby, J. E. *Introduction to Glass Science and Technology*, 2nd ed.; Royal Society of Chemistry: Cambridge, U. K., 2005.

(2) Catlow, C. R. A.; Cormack, A. N.; Theobald, F. *Acta Crystallogr., Sect. B* **1984**, *40*, 195.

(3) Dove, M. T. *Introduction to Lattice Dynamics*; Cambridge University Press: New York, 2005.

(4) Allen, M. P.; Tildsley, D. J. *Computer Simulation of Liquids*; Oxford University Press: Oxford, U. K., 1987.

(5) Oganov, A. R.; Brodholt, J. P.; Price, G. D. *Phys. Earth Planet. Inter.* **2000**, *122*, 277.

(6) Purton, J.; Jones, R.; Catlow, C. R. A.; Leslie, M. *Phys. Chem. Miner.* **1993**, *19*, 392.

(7) Jund, P.; Jullien, R. *Phys. Rev. B* **1999**, *59*, 13707.

(8) Van Beest, B. W. H.; Kramer, G. J.; Van Santen, R. A. *Phys. Rev. Lett.* **1990**, *64*, 1955.

(9) Duffrene, L.; Kieffer J. *J. Phys. Chem. Solids* **1998**, *59*, 1025.

(10) Demilrap E.; Cagin T.; Goddard W. A. *Phys. Rev. Lett.* **1999**, *82*, 1708.

(11) Vashishta, P.; Kalia, R. K.; Rino, J. P.; Ebbsjo, I. *Phys. Rev. B* **1990**, *41*, 12197.

(12) Takada, A.; Richet, P.; Catlow, C. R. A.; Price, G. D. *J. Non-Cryst. Solids* **2004**, *345/346*, 224.

(13) Chagarov, E.; Adams, J. B.; Kieffer, J. *Modell. Simul. Mater. Sci. Eng.* **2004**, *12*, 337.

(14) Huff, N. T.; Demiralp, E.; Cagin, T.; Goddard, W. A., III. *J. Non-Cryst. Solids* **1999**, *253*, 133.

(15) Rappe A. K.; Goddard, W. A., III. *J. Phys. Chem.* **1991**, *95*, 3358.

(16) Wilson, M.; Madden, P. A.; Hemmati, M.; Angell, C. A. *Phys. Rev. Lett.* **1996**, 77, 4023.

(17) Wilson, M.; Madden, P. A.; Costa-Cabral, B. J. *J. Phys. Chem.* **1996**, *100*, 1227.

(18) Wilson, M.; Walsh, T. R. *J. Chem. Phys.* **2000**, *113*, 9180.

(19) Walsh, T. R.; Wilson, M.; Sutton, A. P. *J. Chem. Phys.* **2000**, *113*, 9191.

(20) Tilocca, A.; de Leeuw, N. H.; Cormack, A. N. *Phys. Rev. B* **2006**, *73*, 104209.

(21) *Cerius2*, version 4.2; Accelrys: San Diego, CA, 2000.

(22) Garofalini, S. H. In *Molecular Modelling Theory: Applications in the Geosciences*; Cygan, R. T., Kubicki, J. D., Eds.; Reviews in Mineralogy Geochemistry 42; Geochemical Society, Mineralogical Society of America: Washington, DC, 2001; Chapter 5 and references therein.

(23) Zachariasen, W. H. *J. Am. Chem. Soc.* **1932**, *54*, 3841.

(24) Bush, T. S.; Gale, J. D.; Catlow, C. R. A.; Battle, P. D. *J. Mater. Chem.* **1994**, *4*, 831.

(25) Lewis, G. V.; Catlow, C. R. A. *J. Phys. C: Solid State Phys.* **1985**, *18*, 1149.

(26) Vessal, B.; Amini, M.; Fincham, D.; Catlow, C. R. A. *Philos. Mag. B* **1989**, *60*, 753.

(27) Lusvardi, G.; Malavasi, G.; Menabue, L.; Menziani, M. C. *J. Phys. Chem. B* **2002**, *106*, 9753.

(28) Linati, L.; Lusvardi, G.; Malavasi, G.; Menabue, L.; Menziani, M. C.; Mustarelli, L. P.; Segre, U. *J. Phys. Chem. B* **2005**, *109*, 4989.

(29) Lusvardi, L.; Malavasi, G.; Menabue, L.; Menziani, M. C.; Pedone, A.; Segre, U. *J. Phys. Chem. B* **2005**, *109*, 21586.

(30) Malavasi, G.; Menziani, M. C.; Pedone, A.; Segre, U. *J. Non-Cryst. Solids* **2006**, *352*, 285.

(31) Yuan, X.; Cormack, A. N. *J. Non-Cryst. Solids* **2001**, *283*, 69.

(32) Corradi, A. B.; Cannillo, V.; Montorsi, M.; Siligardi, C.; Cormack, A. N. *J. Non-Cryst. Solids* **2005**, *351*, 1185.

(33) Parker, S. C.; Price G. D. *Adv. Solid State Chem.* **1989**, *1*, 295.

(34) Gale, J. D. *J. Chem. Soc., Faraday Trans.* **1997**, *93*, 629.

(35) Gale J. D. *Philos. Mag. B* **1996**, *73*, 3.

(36) The General Utility Lattice Program by J. Gale can be downloaded from the Web site http://gulp.curtin.edu.au/.

(37) Gale, J. D.; Rohl, A. L. *Mol. Simul.* **2003**, *29*, 291.

(38) Kramer, G. J.; Farragher, N. P.; van Beest, B. W. H.; van Santen, R. A.; *Phys. Rev. B* **1991**, *43*, 5068.

(39) Gale, J. D.; Henson, N. J. *J. Chem. Soc., Faraday Trans.* **1994**, *90*, 3175.

(40) atson, G. W.; Tschaufeser, P.; Wall, A.; Jackson, R. A.; Parker, S. C. In *Computer Modelling in Inorganic Crystallography*; Catlow, C. R. A., Ed.; Academic Press: San Diego, CA, 1997; Chapter 3.

(41) Ney, J. F. *Physical Properties of Crystals*; Oxford Scientific Publications: Oxford, U. K., 1985.

(42) Bakaev, V. A.; Steele, W. A. *J. Chem. Phys.* **1999**, *111*, 9803

(43) Du, J.; Cormack, A. N. *J. Non-Cryst. Solids* **2004**, *349*, 66.

(44) Ewald P. P. *Ann. Phys.* **1921**, *64*, 253.

(45) Leach, A. R. *Molecular Modelling: Principles and Applications*; Prentice Hall: New York, 2001.

(46) Fletcher, R.; Reeves, C. M. *Comput. J.* **1964**, *7*, 149.

(47) Manghnani, M. H. In *Handbook of Glass Properties*; Bansal, N. P., Doremus, R. H., Eds.; Academic Press: London, 1986.

(48) Hwa, L. G.; Hsieh, K. J.; Liu, L. C. *Mater. Chem. Phys.* **2003**, *78*, 105.

(49) *SciGlass, Universal System of Glass Properties*, version 3.5; SciVision: Burlington, MA, 1997 and references therein.

(50) The DL_POLY code by W. Smith and T. R. Forester can be downloaded from the Web site http://www.dl.ac.uk/TCSC/Software/DL_POLY.

(51) Evans, D. J. Morris, G. P. *Comput. Phys. Rep.* **1984**, *1*, 297.

(52) Yuan, X.; Cormack, A. N. *Comput. Mater. Sci.* **2002**, *24*, 343.

(53) Wright, A. C.; Clare, A. G.; Bachra, B.; Sinclair, R. N.; Hannon, A. C.; Vessal, B. *Trans. Am. Crystallogr. Assoc.* **1991**, *27*, 239.

(54) Grimley, D. I.; Wright, A. C.; Sinclair, R. N. *J. Non-Cryst. Solids* **1990**, *119*, 49.

(55) Clare, A. G.; Bachra, B.; Wright, A. C.; Sinclair, R. N. In *The Physics of Non-Crystalline Solids*; Pye, L. D., Lacourse, W. C., Stevens, H. J., Eds.; Taylor and Francis: London, 1992.

(56) Henderson, G. S. *J. Non-Cryst. Solids* **1995**, *183*, 43.

(57) Greaves, G. N.; Fontaine, A.; Lagrarde, P.; Raoux, D.; Gurman, S. J. *Nature* **1981**, *293*, 611.

(58) Mazzara, C.; Jupille, J.; Flank, A. M.; Lagarde, P. *J. Phys. Chem B* **2000**, *104*, 3438.

(59) *Inorganic Crystal Structure Database*, version 1.3.3; National Institute of Standards and Technology: Gaithersburg, MD, 2004 and references therein.

(60) Ozkan, H.; Cartz, L.; Jamieson, J. C. *J. Appl. Phys.* **1974**, *45*, 556.

(61) Lide, D. R. *Handbook of Chemistry and Physics*, 76th ed.; CRC Press: Boca Raton, FL, 1995−1996.

(62) Born, M.; Huang, K. *Dynamical Theory of Crystal Lattices*; Clarendon Press: Oxford, U. K., 1954.

(63) Bass, J. D. Chapter 7 In *Mineral Physics and Crystallography: A Handbook of Physical Constants*; Ahrens, T. J., Ed.; American Geophysical Union: Washington, DC, 1995.

(64) Misawa, M.; Price, D. L.; Suzuki, K. *J. Non-Cryst. Solids* **1980**, *37*, 85.

(65) Poulsen, H. F.; Neuefeind, J.; Neumann, H. B.; Schneider, J. R.; Zeidler, M. D. *J. Non-Cryst. Solids* **1995**, *188*, 63.

(66) Clark, T. M.; Grandinetti, P. J.; Florian, P.; Stebbins, J. F. *Phys. Rev. B* **2004**, *70*, 064202.

Empirical Interatomic Potential Model for Glasses

*J. Phys. Chem. B, Vol. 110, No. 24, 2006* **11795**

(67) Appen, A. A. *Chemistry of Glass*; Khimiya: Leningrad, 1970 (in Russian).

(68) Gan Fuxi *Sci. Sin.* **1974**, *17*, 533.

(69) Demkina, L. I. *Izd. Chimia* **1976**, *23*, 123.

(70) Priven, A. I. *Glass Technol.* **2004**, *45*, 244.

(71) Sierka, M.; Sauer, J. *Faraday Discuss.* **1997**, *106*, 41.

(72) Thong N. G. O.; Schwarzenbach D. *Acta Crystallogr., Sect. A* **1979**, *35*, 658.

(73) Ecolivet, C.; Poignant, H. *Phys. Status Solidi* **1981**, *63*, K107.

(74) Wang, H.; Xu, B.; Liu, X.; Han, J.; Shan, S.; Li, H. *J. Cryst. Growth* **1986**, *79*, 227.

(75) Dick, B. G.; Overhauser, A. W. *Phys. Rev.* **1958**, *112*, 90.

(76) Sanders, M. J.; Leslie, M. J.; Catlow, C. R. A. *J. Chem. Soc., Chem. Commun.* **1984**, 1271.

(77) Pascale, F.; Catti, M.; Damin, A.; Orlando, R.; Saunders: V. R.; Dovesi, R. *J. Phys. Chem B* **2005**, *109*, 18522.

(78) Orlando, R.; Torres, F. J.; Pascale, F.; Ugliengo, P.; Zicovich-Wilson, C.; Dovesi, R. *J. Phys. Chem. B* **2006**, *110*, 692.